Two opposing roles for Bmp signalling in the development of electrosensory lateral line organs

Alexander S. Campbell[1], Martin Minařík[1], Roman Franěk[2], Michaela Vazačová[2], Miloš Havelka[2], David Gela[2], Martin Pšenička[2] and Clare V. H. Baker[1]*

Affiliations:

[1]Department of Physiology, Development & Neuroscience, University of Cambridge, Cambridge, UK

[2]Faculty of Fisheries and Protection of Waters, Research Institute of Fish Culture and Hydrobiology, University of South Bohemia in České Budějovice, Vodňany, Czech Republic

*For correspondence: cvhb1@cam.ac.uk

Abstract

The lateral line system enables all fishes and aquatic-stage amphibians to detect local water movement via mechanosensory hair cells in neuromasts, and many species to detect weak electric fields via electroreceptors (modified hair cells) in ampullary organs. Both neuromasts and ampullary organs develop from lateral line placodes. However, the molecular mechanisms underpinning ampullary organ formation are understudied relative to neuromasts, as the ancestral lineages of zebrafish (teleosts) and *Xenopus* (frogs) independently lost electroreception. We identified *Bmp5* as a promising candidate via differential RNA-seq in an electroreceptive ray-finned fish, the Mississippi paddlefish (*Polyodon spathula*; Modrell et al., 2017, *eLife* 6: e24197). In an experimentally tractable relative, the sterlet sturgeon (*Acipenser ruthenus*), we found that *Bmp5* and four other Bmp pathway genes are expressed in the developing lateral line, and that Bmp signalling is active. Furthermore, CRISPR/Cas9-mediated mutagenesis targeting *Bmp5* in G0-injected sterlet embryos resulted in fewer ampullary organs. Conversely, when Bmp signalling was inhibited by DMH1 treatment shortly before the formation of ampullary organ primordia, supernumerary ampullary organs developed. These data suggest that Bmp5 promotes ampullary organ development, whereas Bmp signalling via another ligand(s) prevents their overproduction. Taken together, this demonstrates two opposing roles for Bmp signalling during ampullary organ formation.

Introduction

The lateral line system is an evolutionarily ancient sensory system found in all fishes and aquatic-stage amphibians (Bullock et al., 1983; Northcutt, 1997; Mogdans, 2021). There are two distinct types of lateral line organs in the skin. Neuromasts, arranged in characteristic lines across the head and trunk, detect local water movement via mechanosensory hair cells ("touch at a distance") whose apical surfaces are embedded in a gelatinous cupula (Cernuda-Cernuda and García-Fernández, 1996; Montgomery et al., 2014; Pickett and Raible, 2019; Mogdans, 2021). In non-teleost electroreceptive fishes and amphibians, fields of electrosensory ampullary organs flank some or all of the neuromast lines on the head (Bullock et al., 1983; Baker et al., 2013; Crampton, 2019). The electrosensory division of the lateral line system was independently lost in several lineages, for example, those leading to frogs/toads and to teleost fishes (although electroreception with physiologically distinct electroreceptors independently evolved multiple times in a few groups of teleost fishes) (Bullock et al., 1983; Baker et al., 2013; Crampton, 2019). Although salamanders (for example, the axolotl) are electroreceptive, the primary anamniote lab models, *Xenopus* and zebrafish, as well as other lab model teleosts such as medaka and cavefish, only have the mechanosensory division.

Non-teleost ampullary organs have a ‘flask-shaped’ chamber with a sensory epithelium at the base, connected to a pore in the epidermis via a canal filled with an electrically conductive jelly (Jørgensen, 2011; Josberger et al., 2016; Zhang et al., 2018). Ampullary electroreceptor cells are modified hair cells (Jørgensen, 2005; Baker and Modrell, 2018; Baker, 2019) that respond to weak cathodal (exterior-negative) electric fields, primarily for detecting prey or avoiding predators (Bodznick and Montgomery, 2005; Crampton, 2019; Leitch and Julius, 2019; Chagnaud et al., 2021). Both neuromasts and ampullary organs contain several types of support cells that flank the sensory receptor cells: these have a range of support functions including secretion (see, for example, Cernuda-Cernuda and García-Fernández, 1996; Camacho et al., 2007; Russell et al., 2022). In zebrafish neuromasts, both active and quiescent stem cell populations have been identified amongst the various support cell populations, which differentiate into hair cells during homeostasis and after injury (see Lush and Piotrowski, 2014; Lush et al., 2019; Undurraga et al., 2019).

Neuromasts, ampullary organs and their afferent neurons all develop from a series of lateral line placodes (thickened patches of neurogenic ectoderm) on the head (Northcutt, 1997; Piotrowski and Baker, 2014; Baker, 2019). There are six bilateral pairs of lateral line placodes: the anterodorsal, anteroventral and otic lateral line placodes form rostral to the otic vesicle, whereas the middle, supratemporal and posterior lateral line placodes form caudal to the otic vesicle (Northcutt, 1997; Piotrowski and Baker, 2014; Baker, 2019). Neuroblasts

delaminate from the pole of each placode lying closest to the otic vesicle; they form afferent bipolar neurons (which coalesce in lateral line ganglia) whose peripheral axons accompany the placode as it continues to develop and form sensory organs (see Piotrowski and Baker, 2014; McGraw et al., 2017; Chitnis, 2021).

Neuromasts on the trunk originate from the posterior lateral line placode, whose development has been most intensively studied in the teleost zebrafish (see, for example, Piotrowski and Baker, 2014; McGraw et al., 2017; Chitnis, 2021). Initially it gives rise to an early-migrating primordium (primI) that migrates as a cell-collective along the trunk, depositing neuromasts and a line of interneuromast cells that act as progenitors for later-forming neuromasts (reviewed by Piotrowski and Baker, 2014). A day later, another placode develops in the same position, which gives rise to two primordia: primD migrates dorsally to give rise to a dorsal line of neuromasts; the other (primII) migrates along the same pathway as primI, depositing secondary neuromasts in between the primary neuromasts left behind by primI (reviewed by Piotrowski and Baker, 2014). The migrating posterior lateral line primordium is closely followed by the growth cones of afferent lateral line axons and their associated Schwann cells (Metcalfe, 1985; Gilmour et al., 2002; Gilmour et al., 2004).

In non-teleosts, the other lateral line placodes do not migrate, but rather elongate over the head to form sensory ridges that eventually fragment, leaving a line of neuromasts along the centre of the ridge (see Winklbauer, 1989; Piotrowski and Baker, 2014). In electroreceptive species, ampullary organs form later than neuromasts, in fields flanking the line of neuromasts (Northcutt, 2005; Baker et al., 2013; Piotrowski and Baker, 2014). Just as in the migrating posterior lateral line primordium, afferent axons and associated Schwann cells accompany the elongating primordia (Winklbauer, 1989; Northcutt, 2005; Piotrowski and Baker, 2014).

Given the loss of electroreception in the lineages leading to frogs/toads and teleosts, we used a chondrostean ray-finned fish, the Mississippi paddlefish (*Polyodon spathula*, which has more ampullary organs than any other species (Chagnaud et al., 2021), as a model to study ampullary organ development (Modrell et al., 2011a; Modrell et al., 2011b; Modrell et al., 2017a; Modrell et al., 2017b; Minařík et al., 2024a). To identify candidate genes potentially involved in ampullary organ development, we performed a differential bulk RNA-seq screen at late-larval stages, comparing gene expression in fin tissue (which lacks lateral line organs) versus operculum tissue (which has many ampullary organs and some neuromasts). This resulted in a lateral line-enriched gene-set containing almost 500 candidate genes enriched by at least two-fold in paddlefish opercular versus fin tissue (Modrell et al., 2017a). Expression analysis of a range of candidate genes from this dataset and other candidates important for hair cell development (Modrell et al., 2017a; Modrell et al., 2017b; Minařík et al., 2024a), together with small-molecule manipulation of the Fgf and Notch signalling pathways (Modrell et al., 2017b), suggested that electoreceptors are closely related to hair cells and that the

mechanisms underlying their development are highly conserved. To enable further investigation of gene function in ampullary organ and electroreceptor development, we moved to a more experimentally tractable chondrostean with a much longer spawning season: a small sturgeon, the sterlet (*Acipenser ruthenus*). Investigation of additional candidate genes from the paddlefish lateral line-enriched dataset in paddlefish and sterlet identified both mechanosensory-restricted and electrosensory-restricted transcription factor gene expression (Modrell et al., 2017a; Minařík et al., 2024a). We recently used CRISPR/Cas9-mediated mutagenesis in G0-injected sterlet embryos to identify a conserved requirement for the 'hair cell' transcription factor Atoh1 in electroceptor formation and identified a role for mechanosensory-restricted Foxg1 in blocking ampullary organ formation within neuromast lines (preprint, Minařík et al., 2024b).

One gene present in the paddlefish lateral line-enriched gene set was the Bmp ligand gene *Bmp5* (2.5-fold enriched in late-larval paddlefish operculum versus fin tissue; Modrell et al., 2017a). Here, we aimed to investigate the expression and function of *Bmp5* and Bmp signalling in the formation of sterlet lateral line organs. This led to our uncovering two opposing roles for Bmp signalling in ampullary organ formation.

Results

Bmp5 is expressed early in developing ampullary organs and later in neuromasts

The only Bmp ligand gene in the paddlefish lateral line organ-enriched gene-set was *Bmp5* (2.5-fold enriched in late-larval paddlefish operculum versus fin tissue; Modrell et al., 2017a). Wholemount *in situ* hybridisation (ISH) in sterlet yolk-sac larvae from stage 37 (hatching occurs at stage 36) to the onset of independent feeding at stage 45 (staging according to Dettlaff et al., 1993), revealed the time-course of *Bmp5* expression relative to the maturation of neuromasts and ampullary organs. The latter was shown by ISH for *Cacna1d*, encoding a voltage-gated calcium channel ($Ca_v1.3$) expressed by differentiated hair cells and electroreceptors (and taste-buds, for example on the barbels) (Modrell et al., 2017a; Minařík et al., 2024a). Within each lateral line primordium, neuromasts form before ampullary organs and hair cells differentiate much earlier than electroreceptors (Minařík et al., 2024a).

At stage 37, faint *Bmp5* expression was seen within developing gill filaments but there was no detectable lateral line expression (Figure 1A,B), despite the presence of some differentiated neuromasts (i.e., with *Cacna1d*-expressing hair cells; Figure 1C,D). By stage 40, strong *Bmp5* expression was visible in mature neuromasts as well as ampullary organ primordia (Figure 1E,F; compare with *Cacna1d* expression in Figure 1G,H, which shows that few electroreceptors have differentiated at this stage). At stage 42, *Bmp5* expression was seen in mature ampullary organs but seemed weaker in neuromasts (Figure 1I,J; compare

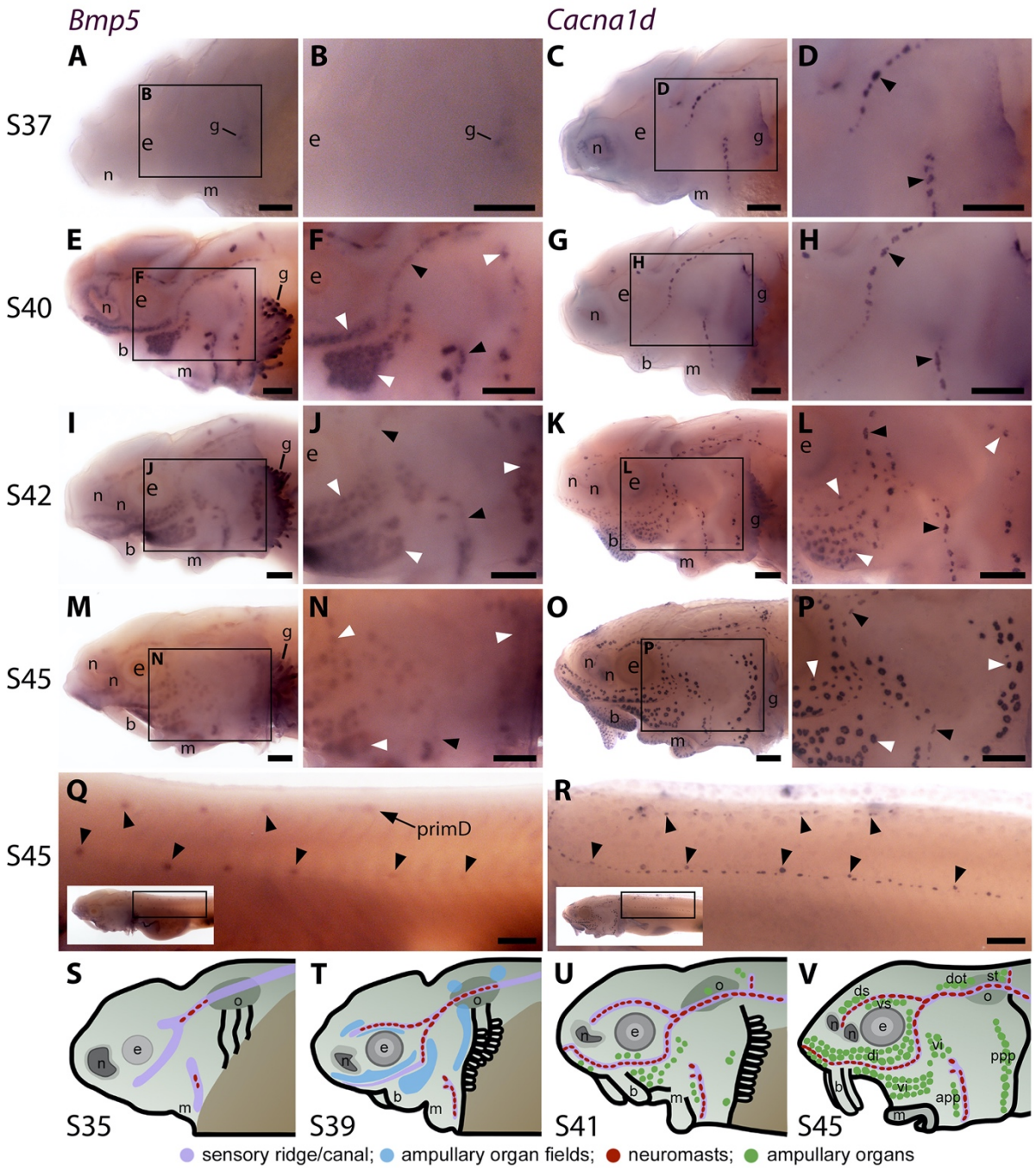

Figure 1. Sterlet *Bmp5* is expressed early in developing ampullary organs and transiently in mature neuromasts. (**A-R**) *In situ* hybridisation in sterlet for *Bmp5* or the hair cell and electroreceptor marker *Cacna1d*, which labels mature neuromasts and ampullary organs (also expressed in taste buds on the barbels). Black arrowheads indicate examples of developing neuromasts; white arrowheads indicate examples of developing ampullary organs. (**A-D**) At stage 37, *Bmp5* expression is only detectable in developing gill filaments (A,B) although *Cacna1d*-positive neuromasts are present (C,D). (**E-H**) At stage 40, *Bmp5* is expressed in neuromasts and ampullary organ primordia (E,F); only a few *Cacna1d*-positive ampullary organs are present at this stage (G,H). (**I-L**) At stage 42, *Bmp5* is expressed in mature ampullary organs and more weakly in neuromasts (I,J); compare with *Cacna1d* expression (K,L). (**M-P**) At stage 45 (onset of independent feeding), *Bmp5* expression is weaker in ampullary organs and no longer detectable in most neuromasts (M,N); compare with *Cacna1d* expression (O,P). (**Q,R**) At stage 45 on the trunk, *Bmp5* expression is visible in primII-deposited secondary neuromasts (more strongly in more rostral neuromasts) as well as in primD and neuromasts of the dorsal line (Q). Compare with *Cacna1d* expression in all neuromasts (R): arrowheads indicate

examples of dorsal-line neuromasts and primII-deposited secondary neuromasts (offset a little dorsal to the line of primI-deposited primary neuromasts). Low-power insets show the location of these trunk regions. (**S-V**) Schematic depictions of sterlet lateral line organ development at similar stages (stages 35, 39, 41, 45), previously published in Minařík et al. (2024a). Abbreviations: app, anterior preopercular ampullary organ field; b, barbel; di, dorsal infraorbital ampullary organ field; dot, dorsal otic ampullary organ field; ds, dorsal supraorbital ampullary organ field; e, eye; gf, gill filaments; m, mouth; n, naris; o, otic vesicle; ppp, posterior preopercular ampullary organ field; prim, migrating lateral line primordium (primI, primary; primII, secondary; primD, dorsal); S, stage; st, supratemporal ampullary organ field; vi, ventral infraorbital ampullary organ field; vs, ventral supraorbital ampullary organ field. Scale bar: 250 µm.

with *Cacna1d* expression in Figure 1K,L). By stage 45, *Bmp5* expression persisted in ampullary organs, although this seemed weaker than at stage 40, and was no longer seen in most neuromasts on the head (Figure 1M,N; compare with *Cacna1d* expression in Figure 1O,P). On the trunk, *Bmp5* expression was seen in a subset of regularly spaced neuromasts in the main body line, as well as the dorsal line deposited by primD, with stronger expression in more rostral (i.e., earlier-deposited) neuromasts (Figure 1Q; compare with *Cacna1d* expression in all trunk neuromasts in Figure 1R). The *Bmp5*-expressing neuromasts in the main body line are secondary neuromasts deposited by the later-migrating primII, which are offset slightly dorsally to those deposited earlier by primI, which are *Bmp5*-negative (compare with *Cacna1d* expression in Figure 1R; examples of primII-deposited neuromasts are highlighted). Figure 1S-V show schematic summaries of cranial neuromast and ampullary organ development at similar stages (from Minařík et al., 2024a).

Overall, these results suggest that *Bmp5* is expressed early within ampullary organ primordia and maintained in mature ampullary organs at least through to the onset of independent feeding at stage 45. In contrast, *Bmp5* only seems to be expressed in mature neuromasts, after the onset of hair cell differentiation, and then only transiently.

The Bmp signalling pathway is active throughout the developing sterlet lateral line system

To investigate where and when the Bmp signalling pathway is active during sterlet lateral line organ development, we performed wholemount immunohistochemistry using an antibody raised against human phospho-SMAD1/5/9 (pSMAD1/5/9; SMAD9 was formerly known as SMAD8), as a proxy for Bmp signalling (Schmierer and Hill, 2007).

At stage 30 (the earliest stage examined), faint pSMAD1/5/9 immunoreactivity was seen in the region of the anteroventral lateral line primordium (Figure 2A,B; compare with Sox2 immunoreactivity at stage 32 in Supplementary Figure S1A,B; Sox2 is expressed in lateral line primordia and maintained in supporting cells; Hernández et al., 2007; Modrell et al., 2017a; Minařík et al., 2024a). By stage 34, pSMAD1/5/9 immunoreactivity was detectable in lateral line primordia, with a ring pattern around developing neuromast primordia in the

otic/anterodorsal and anteroventral primordia (Figure 2C,D; compare with stage 35 Sox2 expression in Supplementary Figure S1C,D). (The first *Cacna1d*-positive differentiated hair cells are seen in this region at stage 35; Minařík et al., 2024a.) At stage 36 (Figure 2E,F), weak pSMAD1/5/9 immunoreactivity was still seen around developing neuromasts (compare with stage 37 *Cacna1d* expression in Figure 1C,D; stage 37 Sox2 immunoreactivity in Supplementary Figure S1E,F), but we were intrigued to see more prominent immunoreactivity in a filamentous pattern that seemed most likely to correspond to lateral line nerves (Figure 2E,F). This pattern continued at stages 38 and 40 (Figure 2G-J); indeed pSMAD1/5/9 immunoreactive collaterals seemed to be developing from the infraorbital nerve between stages 38 and 40 (Figure 2G-J). At stage 40, diffuse immunoreactivity was also seen in regions flanking the nerves where ampullary organ primordia are forming (Figure 2I,J; compare with stage 40 *Bmp5* expression in Figure 1E,F). (Strong pSMAD1/5/9 immunoreactivity was also seen in the barbel primordia, around the nares and mouth, in gill filaments, and between stages 36 and 40 in a patch between the barbels and the otic vesicle that likely represents a muscle, the *m. protractor hyomandibulae*; Warth et al., 2018.)

By stage 42, pSMAD1/5/9 immunoreactivity was visible in ampullary organs and much less prominent in lateral line nerves (Figure 2K,L; compare with stage 42 Sox2 expression in Supplementary Figure S1I,J). At stages 43 and 45, pSMAD1/5/9 immunoreactivity was more clearly visible in neuromasts as well as ampullary organs, in all cases at the periphery rather than centre of each organ (Figure 2M-P; compare with the hair cell/electroreceptor marker *Cacna1d* at stage 42 in Figure 1K,L and at stage 45 in Figure 1O,P, and the supporting cell marker Sox2 at stages 42 and 45 in Supplementary Figure S1I-L). This peripheral pattern of pSMAD1/5/9 immunoreactivity suggests that Bmp signalling is active in supporting cells rather than receptor cells. Also at stages 43 and 45, we noted that pSMAD1/5/9 immunoreactivity on the head seemed to be particularly strong in the supraorbital and infraorbital neuromast lines (compare with Sox2 expression at stages 42 and 45 in Supplementary Figure S1I-L).

pSMAD1/5/9 immunoreactivity was also prominent in the migrating lateral line primordia on the trunk. At stage 39, pSMAD1/5/9 immunoreactivity was seen in primI and a diffuse but somewhat continuous line trailing behind it, as well as in primII, which is located much further rostrally and a little dorsal to the main line (Figure 2Q; compare with Sox2 expression in Figure 2R). At stage 45, strong pSMAD1/5/9 immunoreactivity was seen in primII and primD, and more weakly along the path taken by primII, with increased intensity at the periphery of the primII-deposited neuromasts (Figure 2S; compare with Sox2 expression in all neuromasts in Figure 2T and with *Bmp5* expression in primII-deposited neuromasts in Figure 1Q). (For further comparison, Supplementary Figure S1M-P show the positions of the different migrating primordia on the trunk via Sox2 expression at stages 38, 40, 42 and 45.)

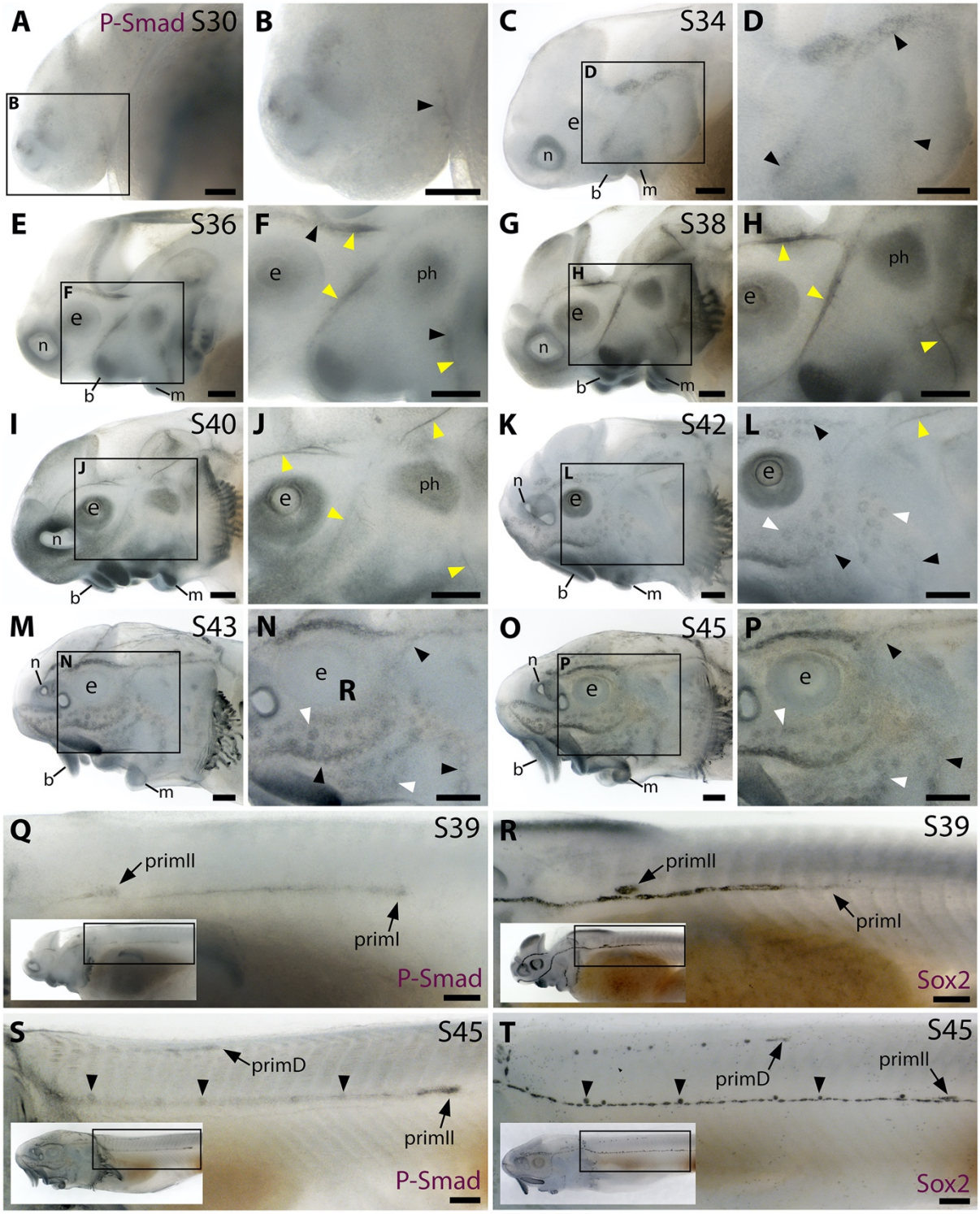

Figure 2. The Bmp signalling pathway is active throughout the developing lateral line system in sterlet. Immunostaining in sterlet. Black arrowheads indicate examples of developing neuromasts; white arrowheads indicate examples of developing ampullary organs; yellow arrowheads indicate lateral line nerves. (**A-P**) Immunoreactivity on the head for phospho-SMAD1/5/9 (P-Smad) as a proxy for Bmp signalling activity. At stage 30 (A,B), weak immunoreactivity is seen in the region of the anteroventral lateral line primordium and by stage 34 (C,D) in lateral line primordia, with a ring pattern around developing neuromast primordia. At stages 36-40 (E-J), immunoreactivity is weak around developing neuromasts and prominent in lateral line nerves (yellow arrowheads). At stage 40 (I,J), diffuse immunoreactivity is also seen in regions flanking the nerves where ampullary organ primordia are forming. Non-lateral line immunoreactivity is present around the mouth and nares, in barbel primordia,

gill filaments, and a patch that is most likely the developing muscle *m. protractor hyomandibulae*. Between stages 42 and 45 (K-P), immunoreactivity disappears in lateral line nerves and is increasingly detected at the periphery of ampullary organs and neuromasts (strongly in supraorbital and infraorbital neuromast lines). (**Q-T**) Immunostaining on the trunk (boxes on low-power insets indicate the location of the trunk regions shown). At stage 39 (Q,R), pSMAD1/5/9 immunoreactivity is seen in primI and a diffuse trail behind it, and in primII (Q). For comparison, Sox2 is expressed weakly in primI and strongly in primI-deposited neuromasts and interneuromast cells, plus primII (R). At stage 45 (S,T), pSMAD1/5/9 immunoreactivity is seen in primD and primII plus a weak trail behind it, with greater intensity at the periphery of primII-deposited neuromasts (S). For comparison, Sox2 expression is strong in primII, primD and all neuromasts; arrowheads indicate examples of primII-deposited neuromasts (T). Abbreviations: b, barbel; e, eye; f, fin; g, gill filaments; m, mouth; n, naris; ph, *m. protractor hyomandibulae*; prim, migrating lateral line primordium (primI, primary; primII, secondary; primD, dorsal); S, stage. Scale bar: 250 µm.

Overall, these data suggest that Bmp signalling is active throughout lateral line development in the sterlet, including lateral line organ primordia and even lateral line nerves, and later at the periphery of maturing ampullary organs and neuromasts, suggesting activity in supporting cells rather than receptor cells.

***Bmp4* is also expressed during sterlet lateral line organ development**

Bmp5 was the only gene encoding a Bmp ligand or receptor in the late-larval paddlefish lateral line-enriched gene-set (Modrell et al., 2017a). However, the timecourse and pattern of pSMAD1/5/9 immunoreactivity in the developing sterlet lateral line system was more extensive than *Bmp5* expression (compare Figures 1 and 2), suggesting other Bmp ligands must be expressed that were not enriched in the transcriptome of late-larval paddlefish operculum versus fin tissue (Modrell et al., 2017a). We therefore searched the pooled larval sterlet transcriptome that was available to us at the time, for additional Bmp pathway ligand and receptor genes for cloning and ISH. This enabled us to examine the expression of the ligand gene *Bmp4* and the type II receptor gene *Acvr2a*. Indeed, after these experiments were underway, a lateral line organ-enriched gene-set from stage 45 Siberian sturgeon (*Acipenser baerii*) was published that included *Bmp4* as well as *Bmp5* (Wang et al., 2020).

Bmp4 expression was not evident in the developing sterlet lateral line at stage 37 or stage 38 (Figure 3A-D); the very faint expression in two widely spaced dorsal patches at stage 38 may be sensory patches in the otic vesicle (Figure 3C,D), or may represent early-forming neuromast primordia in the otic and supratemporal lines (see Gibbs and Northcutt, 2004). Stronger expression was also seen in fin, barbel and gill filament primordia, and around the nares (Figure 3A-D). By stage 40, diffuse *Bmp4* expression was observed in neuromast regions and fields of ampullary organ primordia on the head (Figure 3E,F; compare with *Bmp5* and *Cacna1d* expression in Figure 1E-H). Stronger expression was also seen on the trunk in primI, with much weaker expression in the most recently deposited neuromasts near to the primordium, plus a spot that most likely represents primII (Figure 3G; compare with stage 40

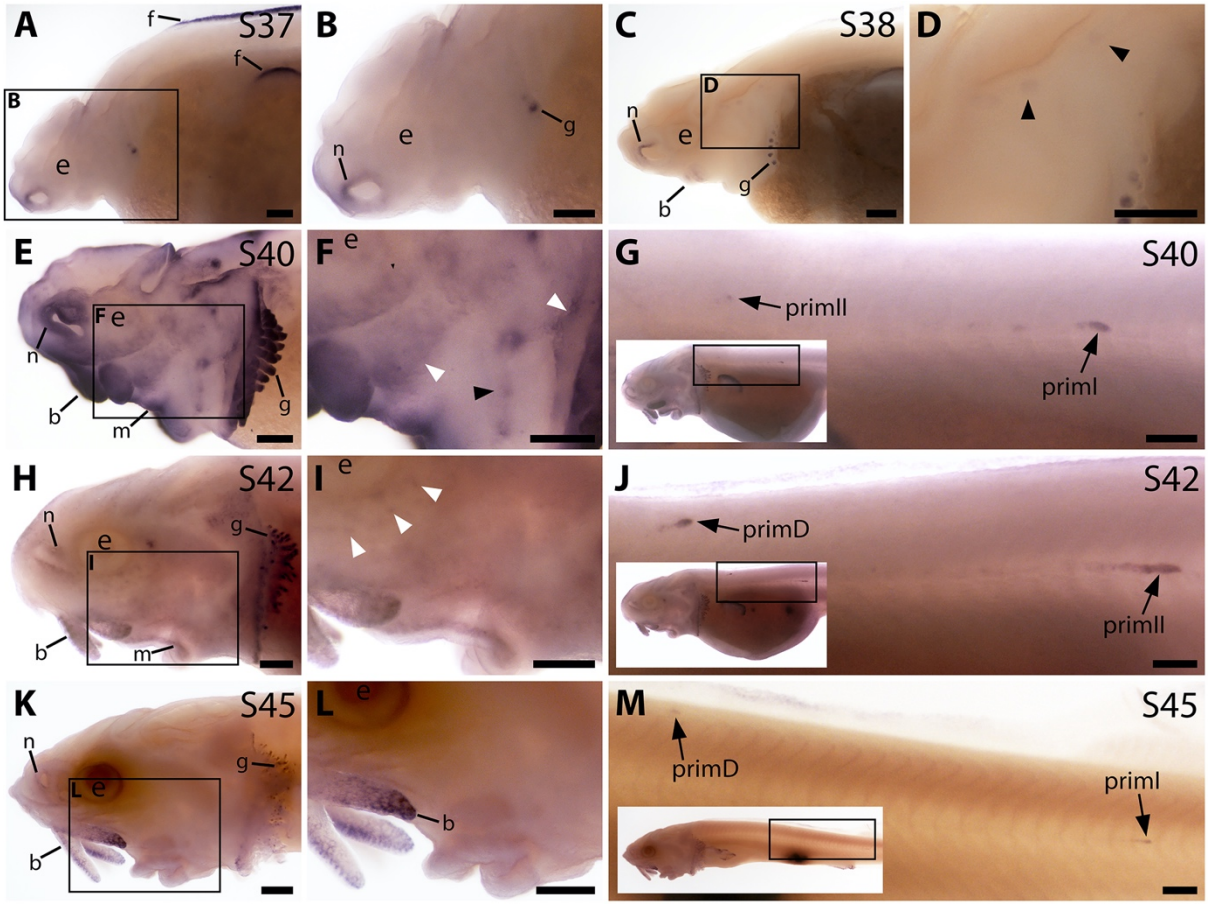

Figure 3. *Bmp4* is expressed transiently during sterlet lateral line organ development. *In situ* hybridisation in sterlet for *Bmp4*. Black arrowheads indicate examples of neuromast regions; white arrowheads indicate examples of ampullary organ regions. For images of the trunk, boxes on low-power insets delineate the location of the trunk regions shown. (**A,B**) At stage 37, *Bmp4* is not expressed in lateral line regions, although it is present around the nares and in fins and gill-filament primordia. (**C,D**) At stage 38, two dorsal spots of weak *Bmp4* expression may represent sensory patches in the otic vesicle or early-forming neuromast primordia in the otic and supratemporal lines. Expression is also present in the gills, nares and barbel primordia. (**E-G**) At stage 40, expression is seen on the head in neuromast regions and fields of ampullary organ primordia (E,F; compare with *Bmp5* and *Cacna1d* expression in Figure 1E-H). On the trunk, *Bmp4* is expressed in primI and the most recently deposited neuromasts behind it, and in primII (G). (**H-J**) At stage 42, *Bmp4* expression on the head has largely disappeared (H,I), apart from weak expression in the dorsal infraorbital field (arrowheads in I), although expression is still seen in gill filaments and barbels. On the trunk, expression is seen in primD and primII (J). (**K-M**) At stage 45, no lateral line expression is seen on the head (K,L), though weak expression persists in primD and primI on the trunk (M). Abbreviations: b, barbel; e, eye; f, fin; g, gill filaments; m, mouth; n, naris; prim, migrating lateral line primordium (primI, primary; primII, secondary; primD, dorsal); S, stage. Scale bar: 250 μm.

Sox2 expression on the trunk in Supplementary Figure S1N). At stage 42, *Bmp4* expression in lateral line regions on the head was almost gone, with only faint expression remaining in the dorsal infraorbital ampullary organ field, just below the eye (Figure 3H,I). However, strong expression was seen in primII and primD on the trunk (Figure 3J; compare with stage 42 Sox2 expression in Supplementary Figure S1O). By stage 45, *Bmp4* was no longer expressed in lateral line regions on the head, although expression remained in the barbels and gills (Figure

3K-L). As at stages 40 and 42, the migrating lateral line primordia on the trunk still expressed *Bmp4* at stage 45 (Figure 3M; compare with stage 45 Sox2 expression in Supplementary Figure S1P).

These data suggest that *Bmp4* likely plays a more transient role than *Bmp5* in lateral line organ development. Furthermore, most likely an as-yet unidentified Bmp ligand gene is expressed in lateral line primordia before either *Bmp5* or *Bmp4*, given that pSMAD1/5/9 immunoreactivity was detectable in lateral line primordia at stage 34 (Figure 2C,D).

The only Bmp receptor gene we examined was *Acvr2a*, encoding ActRIIA (activin A receptor type 2A), a type II Bmp receptor that promiscuously binds multiple ligands including Bmp5 and Bmp4 (Yadin et al., 2016). *Acvr2a* was not expressed at stage 37 (Supplementary Figure S2A,B), so other receptors must be involved in mediating Bmp signalling in lateral line primordia at this and earlier stages (see, for example, pSMAD1/5/9 immunoreactivity at stage 34 and stage 36; Figure 2C-F). By stage 38, although background levels were high, *Acvr2a* expression was detectable in developing neuromast regions (Supplementary Figure S2C,D). By stage 40, *Acvr2a* was expressed at the periphery of ampullary organ primordia and neuromasts on the head (Supplementary Figure S2E,F; compare with stage 40 *Bmp5* and *Cacna1d* expression in Figure 1E-H, and with stage 39 Sox2 expression in Supplementary Figure S1G,H). Also at stage 40, *Acvr2a* was expressed in primI and a trailing line of cells behind it, plus a spot most likely representing primII (Supplementary Figure S2G). This pattern persisted in both the head and trunk at stage 42, with expression now also seen primD and in the rostral trunk neuromasts deposited by primII (Supplementary Figure S2H-J). By stage 45, *Acvr2a* expression appeared to be fading on the head, with only faint expression at the periphery of ampullary organs in a few areas (Supplementary Figure S2K,L). However, expression continued in the trunk neuromast lines (Supplementary Figure S2M). Overall, the *Acvr2a* expression pattern does not fully complement either *Bmp5* or *Bmp4* expression (compare with Figures 1 and 3, respectively), or pSMAD1/5/9 immunoreactivity (Figure 2). Hence, other type II receptor(s), as well of course as type I receptors, must be involved.

Sostdc1 **and** ***Apcdd1*****, encoding secreted dual Bmp/Wnt inhibitors, are expressed during sterlet lateral line organ development**

Three genes encoding secreted Bmp inhibitors were present in the late-larval paddlefish lateral line-enriched gene-set (Modrell et al., 2017a): *Sostdc1*, *Apcdd1* and *Vwr2*. *Vwc2* was 4.5-fold lateral line-enriched (Modrell et al., 2017a), but ISH for this gene in sterlet was unsuccessful so it is not considered further.

Sostdc1 (sclerostin domain-containing 1; also known as Wise, Ectodin) is a secreted antagonist of both the Bmp and Wnt pathways (Tong et al., 2022). *Sostdc1* was 4.2-fold enriched in late-larval paddlefish operculum versus fin tissue (Modrell et al., 2017a). From

stage 36 onwards, *Sostdc1* expression was seen in lines of differentiated neuromasts (and in gill filament primordia) on the head, and from stage 40 onwards, in the migrating primordia and neuromasts on the trunk (Supplementary Figure S3A-M; compare with *Cacna1d* expression in Figure 1 and Sox2 expression in Supplementary Figure 1E-P). At stage 42, *Sostdc1* expression was also detected in ampullary organs (Supplementary Figure S3H,I), but this had already disappeared by stage 45 (Supplementary Figure S3K,L). These data suggest *Sostdc1* plays a persistent role within neuromasts, but any function in ampullary organ development is likely to be transient.

Apcdd1 (adenomatosis polyposis coli down-regulated 1) is also a secreted inhibitor of both the Bmp and Wnt pathways (Vonica et al., 2020). *Apcdd1* was 2.2-fold enriched in late-larval paddlefish operculum versus fin tissue (Modrell et al., 2017a). At stage 36, *Apcdd1* was not expressed in differentiated neuromast lines (Supplementary Figure S4A,B), in contrast to *Sostdc1* at the same stage (Supplementary Figure S3A,B). However, there was some *Apcdd1* expression in the region of the preopercular neuromast line, as well as outside the lateral line system: at the edge of the operculum, near the future barbel region and around the mouth (Supplementary Figure S4A,B). At stage 38, more diffuse *Apcdd1* expression was seen in broader regions (Supplementary Figure S4C,D). By stage 40, expression was visible around ampullary organ primordia and some neuromasts on the head (Supplementary Figure S4E,F), as well as primI and primII on the trunk and a relatively short line of trailing cells behind primI (Supplementary Figure S4G). By stage 42, *Apcdd1* expression on the head had largely resolved to the periphery of ampullary organs and neuromasts (Supplementary Figure S4H,I; compare with stage 42 Sox2 expression in Supplementary Figure S1I,J) and continued in the migrating primordia on the trunk and the short line of trailing cells behind primI (Supplementary Figure S4J). At stage 45, this expression pattern largely persisted, although it seemed to be fading in the ventral infraorbital field (Supplementary Figure S4K,L) and faint expression was also now seen along the main body line, potentially at the periphery of trunk neuromasts (Supplementary Figure S4M; compare with stage 45 Sox2 expression on the trunk in Supplementary Figure S1P).

These data, especially the early, broad expression within ampullary organ fields and seemingly very late upregulation in neuromasts, suggest that Apcdd1 may be more important for ampullary organ development. In contrast, the pattern of *Sostdc1* expression (Supplementary Figure S3) suggests its role may be more prominent during neuromast development. However, given the ability of Apcdd1 and Sostdc1 to inhibit both the Bmp and Wnt pathways (Tong et al., 2022; Vonica et al., 2020), we cannot be sure which of these pathway(s) either of these proteins may be antagonising during sterlet lateral line organ development.

CRISPR/Cas9-mediated targeting of *Bmp5* results in fewer ampullary organs forming

Having established that the Bmp signalling pathway is active throughout lateral line organ development and that genes encoding two Bmp ligands, a type II receptor and two secreted dual Bmp/Wnt antagonists are expressed, we wanted to explore the role of Bmp signalling in lateral line development. *Bmp5* was chosen as a target for CRISPR/Cas9-mediated mutagenesis in G0-injected sterlet embryos owing to its earlier expression in ampullary organ primordia. We recently published our approach to CRISPR/Cas9 in sterlet (preprint, Minařík et al., 2024b). The experiments reported here were undertaken at the same time as those reported in Minařík et al. (2024b, preprint). Different 1-2 cell embryos from some of the same batches were injected with Cas9 protein complexed with different combinations of single-guide (sg) RNAs targeting *Bmp5*. Embryos targeted for the melanin-producing enzyme gene *tyrosinase* (*Tyr*) were used as negative controls: this yields a visible phenotype (i.e., defects in pigmentation), but should not affect other developmental processes (preprint, Minařík et al., 2024b).

Our *Bmp5* sgRNAs (Table 1; Figure 4A) were designed before the first chromosome-level sterlet genome was published (Du et al., 2020). Analysis of this genome showed that, rather than being functionally diploid as previously thought (from microsatellite data; Ludwig et al., 2001), the sterlet genome has retained a high level of tetraploidy, including around 70% of ohnologs (i.e., gene paralogs resulting from the independent whole-genome duplication in the sterlet lineage) (Du et al., 2020). Searching the reference genome (Vertebrate Genomes Project NCBI RefSeq assembly GCF_902713425.1) for *Bmp5* showed that both *Bmp5* ohnologs have been retained, on chromosomes 5 and 6, with 88.87% nucleotide identity in the coding sequence (and 95.60% amino acid identity). All of our *Bmp5* sgRNAs fully match the ohnolog on chromosome 6. Relative to the ohnolog on chromosome 5, sgRNAs 2 and 4 (Table 1; Figure 4A) each have a single-base mismatch, respectively, in positions 7 and 4 of the target sequence (PAM-distal), which should be tolerated (Guo et al., 2014; Rabinowitz and Offen, 2021). However, our sgRNA 1 (Table 1; Figure 4A) has two mismatched bases (at positions 3 and 12 of the target sequence) and sgRNA 3 (Table 1; Figure 4A) has a single-base mismatch at position 20, adjacent to the PAM. Therefore, although we expect all our sgRNAs to target the chromosome 6 ohnolog, it is possible that only sgRNAs 2 and 4 successfully target the chromosome 5 ohnolog (Guo et al., 2014; Rabinowitz and Offen, 2021). Nevertheless, given that all combinations of injected sgRNAs contained either sgRNA 2 or sgRNA 4 (Table 1; Supplementary Table S1) we expect all mixtures to have targeted both *Bmp5* ohnologs.

We targeted *Bmp5* using four different sgRNAs targeting exon 1 (Table 1; Supplementary Figure S5A), injected in three different combinations of 2-3 different sgRNAs across two independent batches of 1-2 cell-stage embryos (Supplementary Table S1). The

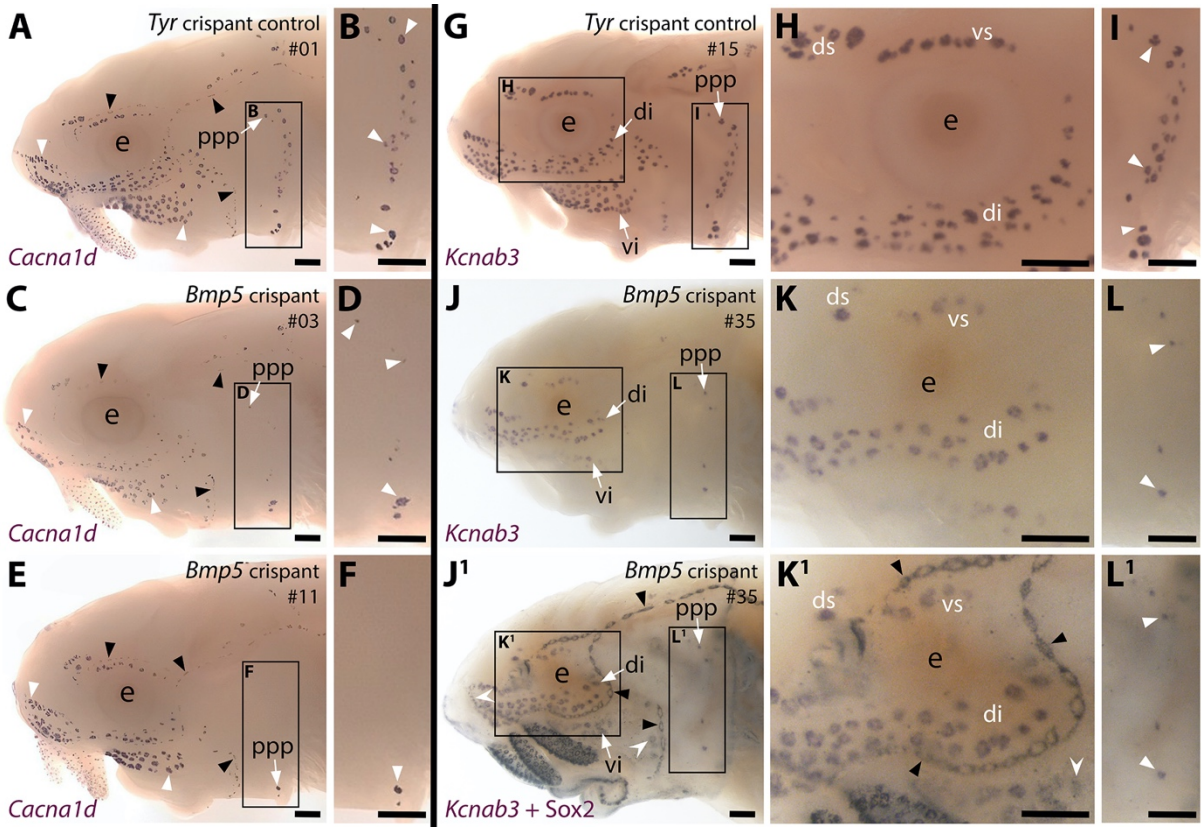

Figure 4. CRISPR/Cas9-mediated targeting of *Bmp5* leads to fewer ampullary organs developing. Sterlet crispants at stage 45 after *in situ* hybridisation (ISH) for the hair cell and electroreceptor marker *Cacna1d* (also expressed in taste buds on the barbels) or the electroreceptor-specific marker *Kcnab3*. All crispants shown are from the same batch of siblings/half-siblings (*in vitro* fertilisation used a mix of sperm from three different males). Black arrowheads indicate examples of neuromasts; white arrowheads indicate examples of ampullary organs. Crispants are numbered for cross-referencing with data provided for each crispant in Supplementary Table S2. (**A,B**) In a control *Tyr* crispant, *Cacna1d* expression shows the normal pattern of neuromast lines flanked by fields of ampullary organs. The higher power view shows the posterior preopercular ampullary organ field. (**C-F**) In *Bmp5* crispants, *Cacna1d* expression reveals fewer ampullary organs (compare C,E with A); this phenotype is particularly prominent in the posterior preopercular ampullary organ field (compare D,F with B). (**G-I**) In a control *Tyr* crispant, electroreceptor-specific *Kcnab3* expression shows the normal distribution of ampullary organs. (**J-L^1**) In a *Bmp5* crispant, *Kcnab3* expression shows fewer ampullary organs (compare J-L with G-I). Post-ISH Sox2 immunostaining for supporting cells (J^1,K^1,L^1) demonstrates that neuromasts have formed normally. Very few "additional" ampullary organs appeared (i.e., Sox2-positive, *Kcnab3*-negative ampullary organs: compare J^1,K^1,L^1 with I,J,K); examples are indicated with indented white arrowheads. (Non-lateral line Sox2 expression is also seen in gill filaments and in taste buds on the barbels and around the mouth.) Abbreviations: di, dorsal infraorbital ampullary organ field; ds, dorsal supraorbital ampullary organ field; e, eye; ppp, posterior preopercular ampullary organ field; S, stage; vi, ventral infraorbital ampullary organ field; vs, ventral supraorbital ampullary organ field. Scale bar: 250 µm.

Bmp5-targeted embryos (hereafter 'crispants') were raised to stage 45 (the onset of independent feeding, approximately 14 days post-fertilisation, dpf). ISH for the hair cell/electroreceptor marker *Cacna1d* (Modrell et al., 2017a; Minařík et al., 2024a) was used to visualise mature neuromasts and ampullary organs (i.e., differentiated hair cells and electroreceptors). Ampullary organ numbers in different fields vary considerably across

individual larvae even in wild-types, but relative to *Tyr* crispants (n=0/30; Figure 4A,B; Supplementary Table S1), we observed a mosaic reduction in *Cacna1d* expression in ampullary organ fields in 46% of *Bmp5* crispants (n=53/116; Figure 4C-F; Supplementary Table S1). The efficacy of different sgRNA combinations varied significantly: injecting sgRNAs 2,3 led to fewer ampullary organs in 78% of cases (n=28/36; Supplementary Table S1) versus 39% for sgRNAs 1,2,3 (n=16/41) and 23% for sgRNAs 1,4 (n=9/39; Supplementary Table S1).

To confirm that our sgRNAs targeted the *Bmp5* locus, we genotyped 43 of the phenotypic *Bmp5* crispants by amplifying the sgRNA-targeted region from trunk/tail genomic DNA by PCR for direct Sanger sequencing. The nature and frequency of edits were analysed by subjecting the Sanger sequence data to *in silico* analysis using Synthego's online 'Inference of CRISPR Edits' (ICE) tool (Conant et al., 2022; also see, for example, Uribe-Salazar et al., 2022). Supplementary Figure S5B shows a control *Tyr* crispant after ISH for *Cacna1d*, for comparison with two of the genotyped *Bmp5* crispants (Supplementary Figure S5C,D). Supplementary Figure S5E-I show examples of ICE output data revealing successful disruption of *Bmp5*; Supplementary Table S2 shows the ICE scores for each crispant analysed. Of the 43 genotyped crispants, 33 had a positive "knock-out" score, confirming successful disruption of the targeted gene (Supplementary Table S2). Our genotyping primers were designed before chromosome-level sterlet genomes were available; comparison with the reference genome (NCBI RefSeq assembly GCF_902713425.1) showed that only the chromosome 6 ohnolog can be amplified, owing to mismatches with the chromosome 5 ohnolog (primarily because the reverse primer targeted an intron). This, combined with crispant mosaicism, may explain why the ICE knock-out score was zero for ten *Bmp5* crispants that nevertheless displayed the phenotype of reduced number of ampullary organs.

To examine the disruption in ampullary organ formation further, 15 control *Tyr* crispants and 13 *Bmp5* crispants (six injected with sgRNAs 2,3 and seven injected with sgRNAs 1,4; Supplementary Table S1) were subjected to ISH for the electroreceptor-specific marker *Kcnab3* (Modrell et al., 2017a; Minařík et al., 2024a). Relative to control *Tyr* crispants (Figure 4G-I), this confirmed the reduction in ampullary organ number when there was no possibility of confusing the two sensory organ types (Figure 4J-L). The same crispants were then immunostained post-ISH for the supporting cell marker Sox2 (Hernández et al., 2007; Modrell et al., 2017a), which labels neuromasts more strongly than ampullary organs (Modrell et al., 2017a; Minařík et al., 2024a) and revealed no obvious phenotype in the number and morphology of neuromasts (Figure 4J^1,K^1,L^1; compare with Figure 4J,K,L). Furthermore, very few "additional" ampullary organs appeared after Sox2 immunostaining (Figure J^1,K^1,L^1; compare with Figure 4J,K,L), suggesting that disrupting the *Bmp5* gene prevented ampullary organ formation, rather than blocking the later differentiation of *Kcnab3*-positive electroreceptors within ampullary organs.

Given the normal variation seen in ampullary organ number in different fields across individual larvae, we wished to test whether the qualitative phenotype of reduced ampullary organ number was statistically significant. We counted all the ampullary organs in each of the eight different fields on one side of the head of 36 phenotypic *Bmp5* crispants after ISH for *Cacna1d* or *Kcnab3*, and 32 control *Tyr* crispants after ISH for *Cacna1d*. The raw counting data are provided in Supplementary Table S2. Statistical analysis using a two-tailed Mann-Whitney (Wilcoxon rank sum) test revealed that *Bmp5* crispants had significantly fewer ampullary organs overall than *Tyr* control crispants ($P<0.0001$; Figure 5A). Indeed, all ampullary organ fields except for the dorsal supraorbital field (one of the smaller fields) had significantly fewer ampullary organs in *Bmp5* crispants versus control *Tyr* crispants (Figure 5B). Figure 5C,D show the location of each of the ampullary organ fields; the colour-coded schematic in Figure 5D also identifies their different lateral line placode origins (based on Gibbs and Northcutt, 2004). The dorsal supraorbital field originates from the anterodorsal lateral line placode, which also gives rise to the ventral supraorbital and the dorsal and ventral infraorbital fields, all of which had significantly fewer ampullary organs in *Bmp5* crispants versus control *Tyr* crispants ($P=0.0008$, $P<0.0001$ and $P<0.0001$, respectively; two-tailed Mann-Whitney test; Figure 5B). Thus, the lack of effect in the dorsal supraorbital field may simply reflect the relatively small number of ampullary organs (although this is not the smallest field).

Overall, these data show that CRISPR/Cas9-mediated targeting of *Bmp5* in G0-injected embryos led to significantly fewer ampullary organs developing in almost all fields. This suggests that *Bmp5*, which is expressed in ampullary organ primordia as well as in mature ampullary organs (Figure 1), normally acts to promote ampullary organ formation.

Blocking Bmp signalling prior to ampullary organ formation results in supernumerary and ectopic ampullary organs

To explore the effect on ampullary organ development of blocking the Bmp pathway more generally than disrupting a specific ligand gene, we used a highly selective small-molecule Bmp inhibitor, DMH1 (dorsomorphin homolog 1) (Hao et al., 2010; Cross et al., 2011). We treated stage 36 (newly hatched) sterlet yolksac larvae with DMH1 for 20 hours, by which point (at 16 °C) they will have reached approximately stage 38, i.e., just prior to the onset of ampullary organ development (ISH for *Eya4* showed that ampullary organ primordia are present in all the main fields by stage 39; Minařík et al., 2024a). In comparison to DMSO controls (n=12), more ampullary organs had formed by stage 45 in all DMH1-treated larvae (n=17/17), as visualised by ISH for the hair cell/electroreceptor marker *Cacna1d* (Figure 6A-D; n=8) or for electroreceptor-specific *Kcnab3* (Figure 6E-H; n=9).

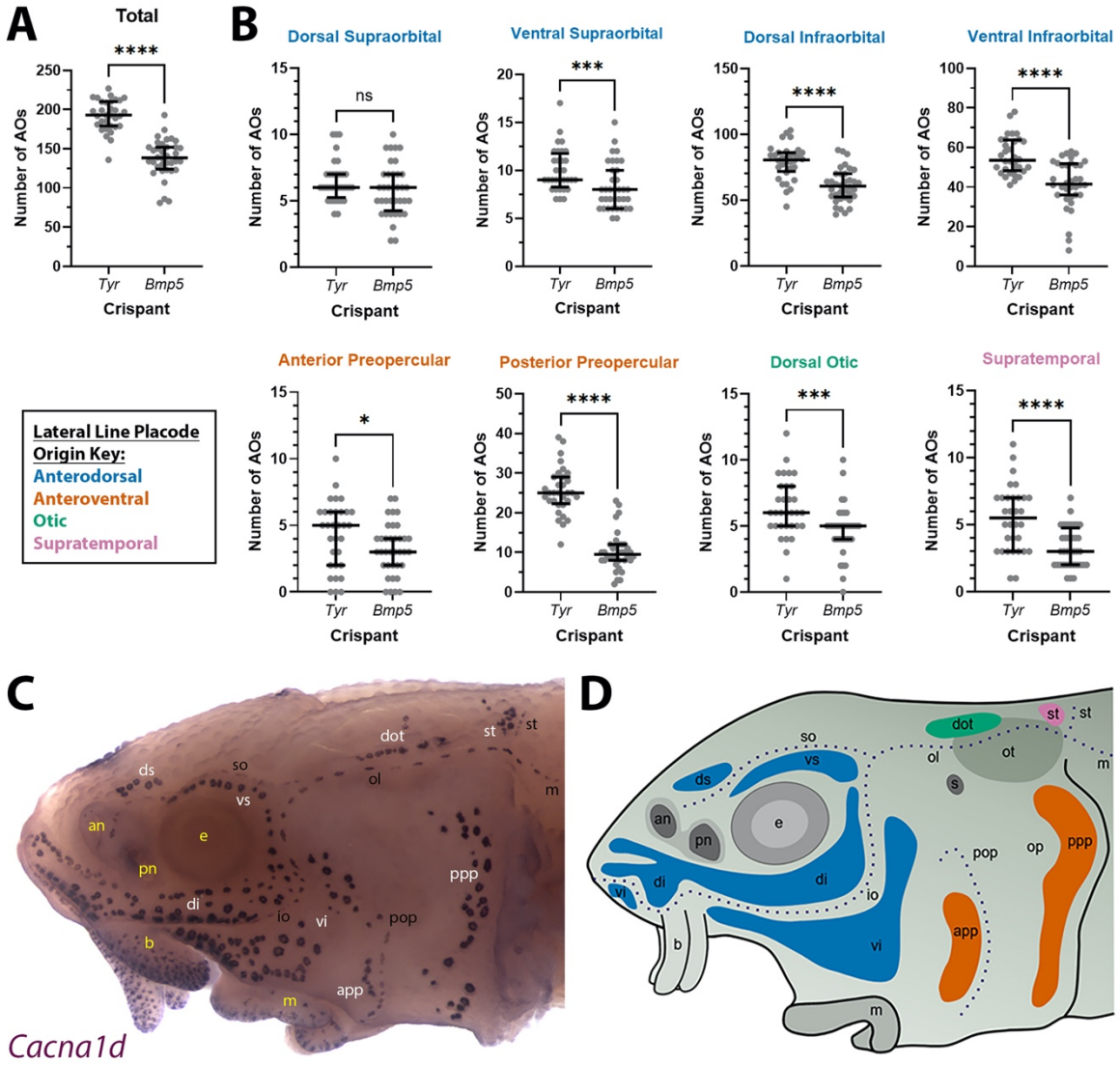

Figure 5. *Bmp5* crispants have significantly fewer ampullary organs than control *Tyr* crispants. (**A**) Scatter plot showing median and interquartile range for the total number of ampullary organs on one side of the head at stage 45 in *Bmp5* sterlet crispants (counted after *in situ* hybridisation [ISH] for *Cacna1d* or *Kcnab3*; n=36) versus control *Tyr* crispants (counted after ISH for *Cacna1d*; n=32). *Bmp5* crispants have significantly fewer ampullary organs overall than control *Tyr* crispants (P<0.0001; two-tailed Mann-Whitney test). Supplementary Table S2 provides the sgRNA combination, injection batch and raw counts for each crispant. All the *Bmp5* crispants and 20 of the *Tyr* crispants used for statistical analysis were from the same batch. (**B**) Scatter plots showing median and interquartile range for the number of ampullary organs in each individual ampullary organ field on one side of the head at stage 45 in *Bmp5* crispants (n=36) versus control *Tyr* crispants (n=32). The raw counts are provided in Supplementary Table S2. For the location of each field, see panel C (*Cacna1d* expression) and panel D (schematic). Scatter plots are grouped with differently coloured titles according to lateral line placode (LLp) origin, following Gibbs and Northcutt (2004): blue, anterodorsal LLp (supraorbital and infraorbital fields); orange, anteroventral LLp (preopercular fields); green, otic LLp (dorsal otic field); pink, supratemporal LLp (supratemporal field). All fields except the dorsal supraorbital field have significantly fewer ampullary organs in *Bmp5* crispants versus control *Tyr* crispants (two-tailed Mann-Whitney tests). Symbols on plots represent P values: ns, not significant, P>0.05; *, P≤0.05; ***, P≤0.001; ****, P≤0.0001. Dorsal supraorbital: not significant, P=0.1207. Ventral supraorbital: P=0.0008. Dorsal infraorbital: P<0.0001. Ventral infraorbital: P<0.0001. Anterior preopercular: P=0.0466. Posterior preopercular: P<0.0001. Dorsal otic: P=0.0008. Supratemporal: P<0.0001. (**C**) Stage 45 sterlet head after ISH for the

hair cell and electroreceptor marker *Cacna1d* (also expressed in taste buds on the barbels). Labels are white for ampullary organ fields; black for neuromast lines; yellow for anatomical landmarks. (**D**) Schematic of a stage 45 sterlet larval head. Ampullary organ fields are represented by coloured patches flanking the neuromast lines, which are represented as dotted lines. The different field colours indicate their lateral line placode origin (consistent with scatter plot titles in B). Abbreviations for ampullary organ fields: app, anterior preopercular; di, dorsal infraorbital; dot, dorsal otic; ds, dorsal supraorbital; ppp, posterior preopercular; st, supratemporal; vi, ventral infraorbital; vs, ventral supraorbital. Abbreviations for neuromast lines: io, infraorbital; m, middle; ol, otic; pop, preopercular; so, supraorbital; st, supratemporal. Abbreviations for anatomical landmarks: an, anterior naris; b, barbel; e, eye; m, mouth; op, operculum; ot, otic vesicle; pn, posterior naris; s, spiracle (first gill cleft).

The increase in ampullary organ number seemed to be general but was most striking in the dorsalmost ampullary organ fields, i.e., the dorsal supraorbital, dorsal otic and supratemporal fields. These fields were clearly separate in the DMSO control larvae (Figure 6A,B,E,F). However, in the DMH1-treated larvae, there were so many ampullary organs that the fields appeared to fuse together in a line (Figure 6C,D,G,H). ISH for *Cacna1d* showed that the three dorsal ampullary organ fields were still clearly separate even in much older larvae (Figure 6I,J), suggesting that the supernumerary ampullary organs in this region of DMH1-treated larvae at stage 45 were ectopic, rather than precocious.

Although the increased number of ampullary organs in the dorsal fields was the most obvious and consistent phenotype, the *Cacna1d* expression pattern in several larvae suggested the presence of ectopic offshoots of the supraorbital neuromast line (Figure 6K,L; n=5/8). Initially, we could not determine from *Cacna1d* expression alone whether the ectopic organs were neuromasts or small ampullary organs, as this gene is expressed by both hair cells and electroreceptors. We therefore took six of the nine larvae that had been subjected to ISH for electroreceptor-specific *Kcnab3* and immunostained them for the supporting cell marker Sox2, which labels neuromasts more strongly than ampullary organs (also see Minařík et al., 2024a). This enabled direct comparison of the same larvae with and without visible neuromasts and showed that the ectopic organs were indeed neuromasts (Figure 6M-N^{1}; n=5/6 as in one larva it was not clear whether an ectopic offshoot was indeed present).

Overall, therefore, ectopic offshoots of the supraorbital neuromast line (compare Figure 6M^{1},N^{1} with wildtype Sox2 expression at stage 45 in Supplementary Figure S1K,L) were seen in a majority of larvae (n=10/14; 71%) in which Bmp signalling had been blocked for 20 hours from stage 36, where this could be determined (n=5/8 after ISH for *Cacna1d*; n=5/6 after ISH for *Kcnab3* followed by immunostaining for Sox2). At stage 36, neuromast primordia are already forming in the supraorbital primordium (as shown by Sox2 expression; Supplementary Figure S1E,F). At stages 36-38, immunoreactivity for pSMAD1/5/9 suggests that Bmp signalling is most prominent in this region in lateral line nerves, rather than the supraorbital lateral line primordium (Figure 2E-H). This suggests the intriguing hypothesis that the Bmp signalling activity during stages 36-38 (the approximate period of DMH1 treatment)

that is required to prevent ectopic secondary neuromast formation from the supraorbital neuromast line, might be active in lateral line nerves, rather than the lateral line primordium itself.

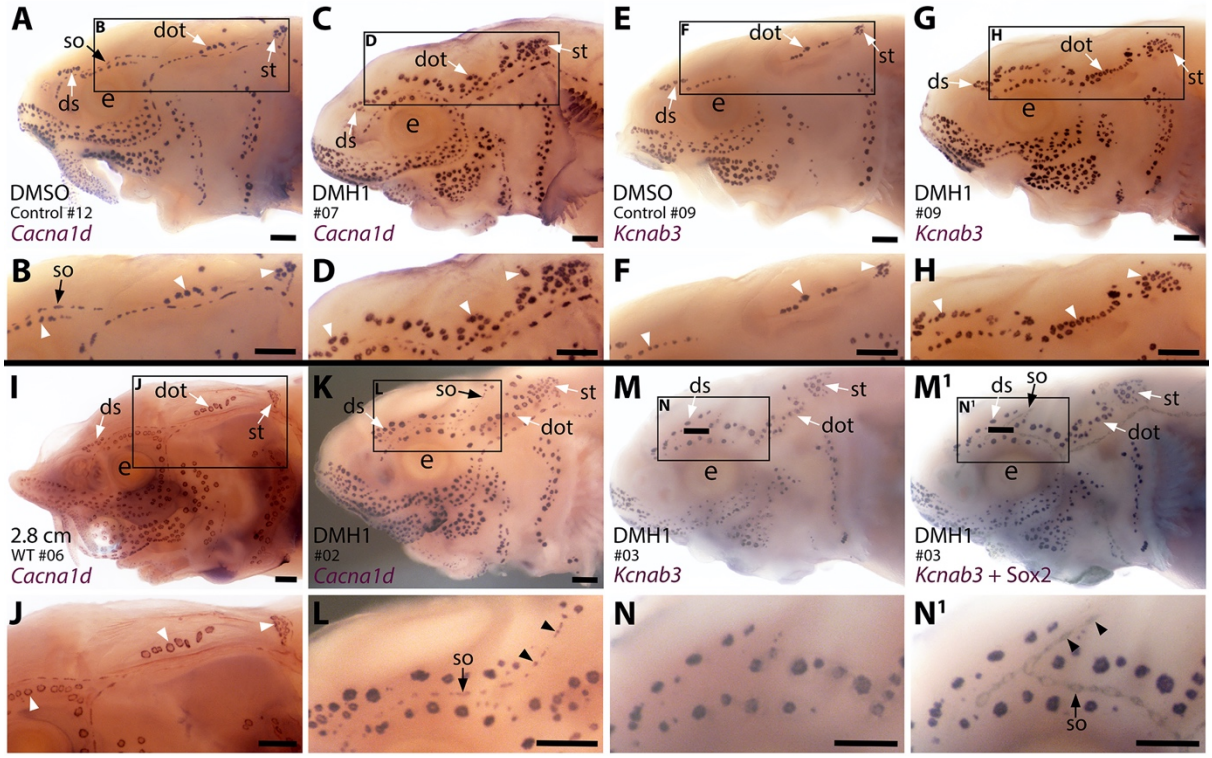

Figure 6. Sterlet larvae in which Bmp signalling was blocked prior to ampullary organ formation have supernumerary ampullary organs and ectopic supraorbital neuromasts. Sterlet larvae after *in situ* hybridisation (ISH) for the hair cell and electroreceptor marker *Cacna1d* (also expressed in taste buds on barbels) or the electroreceptor-specific marker *Kcnab3*. Black arrowheads indicate examples of neuromasts; white arrowheads indicate examples of ampullary organs. (**A-H**) Stage 45 larvae that had been treated for 20 hours from stage 36 (i.e., from hatching to approximately stage 38, just prior to the onset of ampullary organ development) with either DMH1 or DMSO as controls. Larvae are numbered for cross-referencing with ampullary organ counts in Supplementary Table S3. ISH for *Cacna1d* (A-D) or *Kcnab3* (E-H) shows that, relative to DMSO-treated controls (A,B,E,F), DMH1-treated larvae have many more ampullary organs (C,D,G,H). This phenotype is particularly prominent in the three dorsal-most ampullary organ fields, where the dorsal supraorbital, dorsal otic and supratemporal fields - clearly separate in DMSO-treated larvae (A,B,E,F) - almost fuse together in DMH1-treated larvae (C,D,G,H). (**I,J**) A much older wild-type larva (2.8 cm in length, ~65 dpf) after ISH for *Cacna1d*. The dorsal supraorbital, dorsal otic and supratemporal ampullary organ fields are clearly separated, suggesting the supernumerary ampullary organs in this region in DMH1-treated larvae (C,D,G,H) are ectopic, not precocious. (**K-N^1**) Most DMH1-treated larvae also develop an ectopic offshoot from the supraorbital neuromast line. This is visible after ISH for *Cacna1d* (K,L; compare with DMSO control in A,B) and confirmed to represent neuromasts in DMH1-treated larvae via ISH for electroreceptor-specific *Kcnab3* (M,N) followed by immunostaining for the supporting cell marker Sox2 to reveal neuromasts (M^1,N^1). Abbreviations: dot, dorsal otic ampullary organ field; ds, dorsal supraorbital ampullary organ field; e, eye; S, stage; so, supraorbital neuromast line; st, supratemporal ampullary organ field; WT, wild type. Scale bar: 250 µm.

Finally, given the normal variation seen in ampullary organ number in different fields across individual larvae, we wished to test whether the qualitative phenotype of increased ampullary organ number at stage 45 in DMH1-treated versus DMSO control larvae was statistically significant. This included in other ampullary organ fields besides the dorsalmost fields where supernumerary, ectopic ampullary organs were obvious (Figure 6A-K). We therefore counted all the ampullary organs in each of the eight different fields on one side of the head of the stage 45 DMH1-treated larvae (n=17), stage 45 DMSO control larvae (n=12) and older wild-type larvae (either 2.0 cm or 2.8 cm in length, i.e., approximately 50 or 65 dpf; n=10). Supplementary Table S3 shows the raw counting data. Statistical analysis using a two-tailed Mann-Whitney (Wilcoxon rank sum) test confirmed that DMH1-treated larvae had significantly more ampullary organs overall than DMSO controls ($P<0.0001$; Figure 7A). This was also the case for each individual ampullary organ field (Figure 7B; Supplementary Table S3). The colour-coded schematic in Figure 7C shows the location of each field and their different lateral line placode origins (based on Gibbs and Northcutt, 2004).

Furthermore, the DMH1-treated larvae (n=17) had significantly more ampullary organs than older (2.0/2.8 cm) wild-type larvae (n=10), both overall ($P<0.0001$; Figure 8A) and in all fields except the ventral supraorbital and posterior preopercular fields (Figure 8B; Supplementary Table S3; the same colour-coded schematic is shown in Figure 8C). (Note: the five 2.0 cm and five 2.8 cm wild-type larvae were grouped together for statistical comparison with DMH1-treated larvae because using a two-tailed Mann-Whitney test showed that there was no significant difference between ampullary organ numbers in 2.0 cm versus 2.8 cm larvae, either overall [$P=0.4206$] or in any individual field [$P>0.05$ for each field].)

Overall, these results show that blocking Bmp signalling for 20 hours from stage 36, before the first ampullary organ primordia form, results in supernumerary ampullary organs in all fields. Furthermore, ectopic ampullary organs form in the dorsalmost fields, and an ectopic offshoot of the supraorbital neuromast line develops in a majority of larvae. This suggests that during normal development, Bmp signalling dampens ampullary organ formation, preventing the over-production of ampullary organs in each individual field and the formation of ectopic ampullary organs in the most dorsal fields.

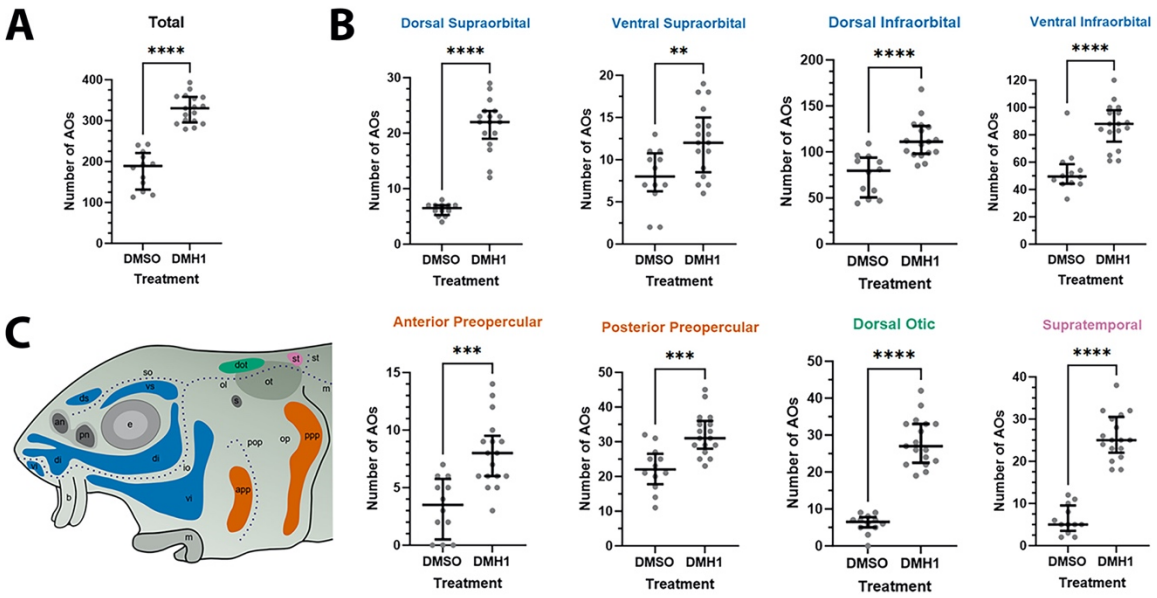

Figure 7. DMH1-treated larvae have significantly more ampullary organs than DMSO controls. (**A**) Scatter plot showing median and interquartile range for the total number of ampullary organs on one side of the head in stage 45 sterlet larvae that had been treated for 20 hours from stage 36 (i.e., from hatching to approximately stage 38, just prior to the onset of ampullary organ development) with DMH1 (n=17) or DMSO as controls (n=12). DMH1-treated larvae have significantly more ampullary organs (P<0.0001; two-tailed Mann-Whitney test). Ampullary organs were counted after *in situ* hybridisation [ISH] for *Cacna1d* or *Kcnab3*; raw counts are provided in Supplementary Table S3. (**B**) Scatter plots showing median and interquartile range for the number of ampullary organs in each individual ampullary organ field on one side of the head in stage 45 sterlet larvae that had been treated for 20 hours from stage 36 with DMH1 (n=17), versus with DMSO as controls (n=12). Raw counts are provided in Supplementary Table S3. For the location of each field, see schematic in panel C (reproduced from Figure 5D). Scatter plots are grouped with differently coloured titles according to lateral line placode (LLp) origin, following Gibbs and Northcutt (2004): blue, anterodorsal LLp origin (supraorbital and infraorbital fields); orange, anteroventral LLp origin (preopercular fields); green, otic LLp origin (dorsal otic field); pink, supratemporal LLp origin (supratemporal field). All fields have significantly more ampullary organs in DMH1-treated larvae (n=17) than in DMSO controls (two-tailed Mann-Whitney tests). Asterisks on plots represent P values: **, P≤0.01; ***, P≤0.001; ****, P≤0.0001. P values for all fields are <0.0001 except for the ventral supraorbital field (P=0.0074), anterior preopercular field (P=0.0002) and posterior preopercular field (P=0.0003). (**C**) Schematic of a stage 45 sterlet larval head. Ampullary organ fields are represented by coloured patches flanking the neuromast lines, which are represented as dotted lines. The different field colours indicate their lateral line placode origin (consistent with scatter plot titles in B). Abbreviations for ampullary organ fields: app, anterior preopercular; di, dorsal infraorbital; dot, dorsal otic; ds, dorsal supraorbital; ppp, posterior preopercular; st, supratemporal; vi, ventral infraorbital; vs, ventral supraorbital. Abbreviations for neuromast lines: io, infraorbital; m, middle; ol, otic; pop, preopercular; so, supraorbital; st, supratemporal. Abbreviations for anatomical landmarks: an, anterior naris; b, barbel; e, eye; m, mouth; op, operculum; ot, otic vesicle; pn, posterior naris; s, spiracle (first gill cleft).

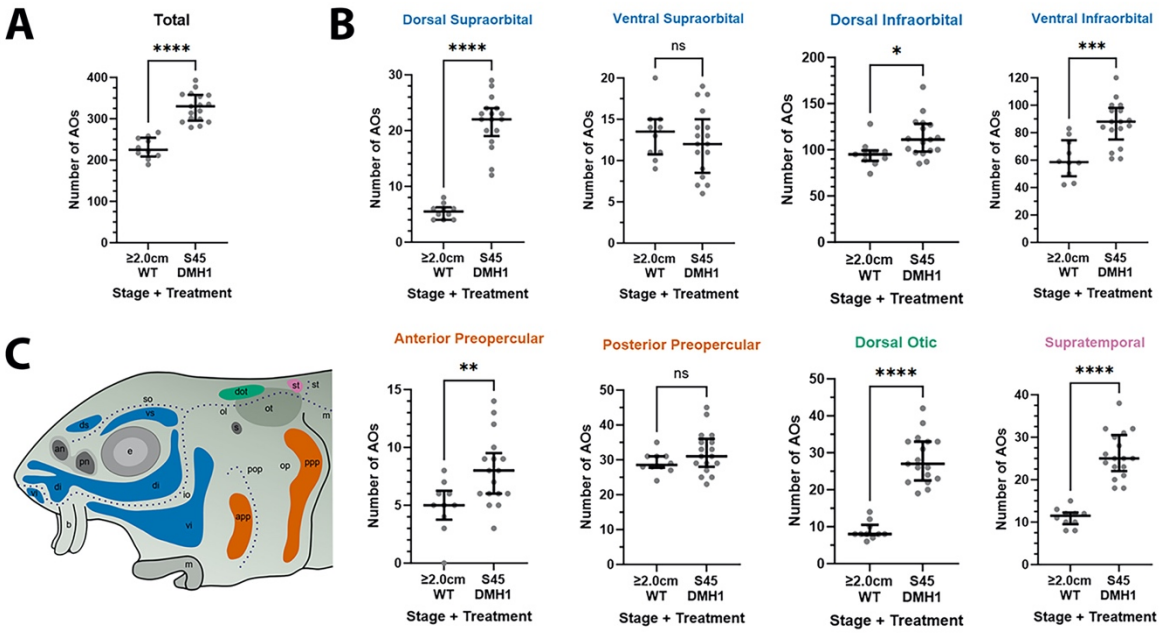

672
673 **Figure 8. DMH1-treated larvae have significantly more ampullary organs at stage 45 than older**
674 **wild-type larvae.** (**A,B**) Scatter plots showing median and interquartile range for the number of
675 ampullary organs on one side of the head in stage 45 sterlet larvae that had been treated for 20 hours
676 from stage 36 with DMH1 (n=17) versus 2.0/2.8 cm wild-type larvae (~50/65 dpf; n=10). Raw counts
677 are provided in Supplementary Table S3. Two-tailed Mann-Whitney tests were used for statistical
678 analysis. DMH1-treated larvae have significantly more ampullary organs overall at stage 45 than wild-
679 type older larvae (P<0.0001; A). In B, scatter plots are grouped with differently coloured titles according
680 to lateral line placode (LLp) origin, following Gibbs and Northcutt (2004): blue, anterodorsal LLp
681 (supraorbital and infraorbital fields); orange, anteroventral LLp (preopercular fields); green, otic LLp
682 (dorsal otic field); pink, supratemporal LLp (supratemporal field). DMH1-treated larvae have significantly
683 more ampullary organs at stage 45 than older wild-type larvae in all fields except the ventral supraorbital
684 and posterior preopercular fields. Symbols on plots represent P values: ns, not significant, P>0.05; *,
685 P≤0.05; **, P≤0.01; ***, P≤0.001; ****, P≤0.0001). Dorsal supraorbital: P<0.0001. Ventral supraorbital:
686 not significant (P=0.5109). Dorsal infraorbital: P=0.0123. Ventral infraorbital: P=0.0002. Anterior
687 preopercular: P=0083. Posterior preopercular: not significant (P=0.1789). Dorsal otic: P<0.0001.
688 Supratemporal: P<0.0001. (**C**) Schematic of a stage 45 sterlet larval head. Ampullary organ fields are
689 represented by coloured patches flanking the neuromast lines, which are represented as dotted lines.
690 The different field colours indicate their lateral line placode origin (consistent with scatter plot titles in
691 B). Abbreviations for ampullary organ fields: app, anterior preopercular; di, dorsal infraorbital; dot, dorsal
692 otic; ds, dorsal supraorbital; ppp, posterior preopercular; st, supratemporal; vi, ventral infraorbital; vs,
693 ventral supraorbital. Abbreviations for neuromast lines: io, infraorbital; m, middle; ol, otic; pop,
694 preopercular; so, supraorbital; st, supratemporal. Other abbreviations: an, anterior naris; b, barbel; e,
695 eye; m, mouth; op, operculum; ot, otic vesicle; pn, posterior naris; s, spiracle (first gill cleft); WT, wild
696 type.
697

Discussion

In this study, we identified two opposing roles for Bmp signalling in ampullary organ development in sterlet. We began by investigating *Bmp5*, the only Bmp ligand gene in our late-larval paddlefish lateral line organ-enriched gene-set (Modrell et al., 2017a). In sterlet, *Bmp5* proved to be expressed in ampullary organ primordia (though not neuromast primordia), as well as in mature ampullary organs and neuromasts. Significantly fewer ampullary organs formed when *Bmp5* was targeted for CRISPR/Cas9-mediated mutagenesis in G0-injected sterlet embryos, suggesting that during normal development, Bmp5 promotes ampullary organ formation. In contrast, blocking Bmp signalling globally at stages just prior to the onset of ampullary organ development led to significantly more ampullary organs forming in all fields. Hence, Bmp signalling activity is required to prevent too many ampullary organs from developing. Taken together, therefore, our study has uncovered dual, opposing roles for Bmp signalling in ampullary organ formation.

Bmp5 promotes ampullary organ formation in sterlet

The early expression of *Bmp5* in ampullary organ primordia, but not neuromast primordia, suggested a role specifically in ampullary organ development. Indeed, targeting *Bmp5* for CRISPR/Cas9-mediated mutagenesis in G0-injected sterlet embryos led to significantly fewer ampullary organs forming, with no effect on neuromast formation. Its precise function in this promoting ampullary organ formation remains to be determined.

In zebrafish, *Bmp5* expression has been reported in the migrating posterior lateral line primordium (Thisse and Thisse, 2004), which also expresses *Bmp4b* and *Bmp2a* (Mowbray et al., 2001). However, a role for Bmp signalling in neuromast development has not been identified (see, for example, Piotrowski and Baker, 2014; Chitnis, 2021). Small-molecule inhibition of Bmp signalling from late epiboly or neural plate stages led to expansion of the posterior (but not pre-otic) lateral line placode, suggesting that a much earlier phase of Bmp signalling restricts the posterior lateral line placode from expanding both posteriorly and laterally (Nikaido et al., 2017).

Bmp5 was also expressed at later stages in ampullary organs and transiently in neuromasts, after electroreceptors/hair cells have differentiated. In mature neuromasts in zebrafish (at 5 dpf), scRNA-seq data show that *Bmp5* is expressed in neuromast hair cell progenitor populations and downregulated as hair cells differentiate (Lush et al., 2019). Furthermore, *Bmp5* is among the genes upregulated in 5-dpf zebrafish neuromasts within one hour after neomycin-induced hair cell death (Jiang et al., 2014; Heller et al., 2022), and in the postnatal mouse cochlea after gentamycin-induced hair cell death (Bai et al., 2019). Hence, Bmp5 may be important for hair cell regeneration. Neomycin treatment at late-larval stages

(stages 44/45) in the Siberian sturgeon (*A. baerii*) kills electroreceptors, as well as hair cells, both of which subsequently regenerate (Fan et al., 2016; Wang et al., 2020). Given the expression of *Bmp5* in mature ampullary organs and neuromasts in sterlet, Bmp5 could play a role in the homeostasis (and regeneration after injury) of electroreceptors as well as hair cells.

Bmp signalling prevents supernumerary and ectopic ampullary organs from forming

In addition to *Bmp5* expression in developing ampullary organ primordia (but not neuromast primordia) and mature ampullary organs and neuromasts, we also identified diffuse, more transient *Bmp4* expression between stages 40-42 within developing ampullary organ fields and neuromast regions. Persistent expression was also seen in the migrating lateral line primordia on the trunk, consistent with a report of *Bmp4b* (as well as *Bmp2a*) expression in the migrating posterior lateral line primordium (primI) in zebrafish (Mowbray et al., 2001). Additional unidentified Bmp ligand(s) are also likely to be expressed in sterlet, as pSMAD1/5/9 immunoreactivity (a proxy for Bmp signalling pathway activity; Schmierer and Hill, 2007) was seen throughout lateral line development, including within elongating lateral line primordia and afferent lateral line nerves (which extend together with all lateral line primordia as they elongate or migrate; Winklbauer, 1989; Northcutt, 2005; Piotrowski and Baker, 2014), as well as at the periphery of developing ampullary organs and neuromasts.

We identified a role for Bmp signalling in preventing too many ampullary organs from forming, using the selective Bmp pathway inhibitor DMH1 (Hao et al., 2010). DMH1 blocks signalling through the type I receptors Acvr1 (Alk2), Acvrl1 (Alk1) and Bmpr1a (Alk3) (Hao et al., 2010; Cross et al., 2011), all of which signal via Smad1/5/8 (Yadin et al., 2016). Acvr1 (Alk2) binds Bmp5/6/7/8; Acvrl1 (Alk1) binds Bmp9/10, and Bmpr1a (Alk3) binds Bmp2/4/5/6/7/8 and Gdf5/6/7 (also known as Bmp14/13/12) (Yadin et al., 2016). We blocked Bmp signalling globally in sterlet yolksac larvae just before the onset of ampullary organ development, by treating them with DMH1 for 20 hours from stage 36 (hatching) to approximately stage 38. By the onset of independent feeding at stage 45, significantly more ampullary organs had formed in all fields relative to DMSO controls, and ectopic ampullary organs had formed in the three dorsalmost fields (the dorsal supraorbital, dorsal otic and supratemporal fields), in regions where ampullary organs are not seen even in much older post-feeding larvae. This suggests Bmp signalling normally prevents supernumerary and ectopic ampullary organs from forming.

Although a role for Bmp signalling has not been identified in neuromast formation (see, for example, Piotrowski and Baker, 2014; Chitnis, 2021), this pathway is important for the formation of inner-ear sensory patches, within which hair cells also differentiate. *Bmp4* is an early marker for all sensory patches in the chicken inner ear, and for the cristae (vestibular

sensory patches of the semicircular canals) in mouse (Wu and Oh, 1996; Morsli et al., 1998). Conditional knockout experiments showed that *Bmp4* is required for the formation of the cristae (Chang et al., 2008). *Bmp4* is also expressed in the developing cochlea, and conditional knockout of the type I receptor genes *Bmpr1a* (*Alk3*) and *Bmpr1b* (*Alk6*) showed that Bmp signalling is also required for the induction of the cochlear-duct prosensory domain that forms the organ of Corti (Ohyama et al., 2010).

Treatment of cultured mouse otocysts with different concentrations of Bmp4 revealed that intermediate levels of Bmp4 promote hair cell formation (Ohyama et al., 2010). Conflicting results were reported from Bmp4 treatment of chicken otocysts explanted at embryonic day 3-4: this either increased hair cell number (Li et al., 2005) or reduced the size of *Atoh1*-positive sensory patches and increased cell death (Pujades et al., 2006). Ohyama et al. (2010) suggested that the differences seen could reflect the concentrations of Bmp4 used being lower (hair cell-promoting; Li et al., 2005) versus higher (hair cell-inhibiting; Pujades et al., 2006). A subsequent study of developing chicken cristae found that both *Bmp4* expression and pSmad1/5/8 immunoreactivity (a proxy for Bmp signalling) were high in most cells of the cristae except in differentiating hair cells, where both were downregulated (Kamaid et al., 2010). In contrast, in the mature (post-hatching) chicken auditory epithelium (basilar papilla), *Bmp4* was highly expressed in hair cells but not supporting cells, and type I receptor genes (*Bmpr1a*, *Bmpr1b*) and a type II receptor gene (*Bmpr2*) were expressed in both hair cells and supporting cells (Lewis et al., 2018). After killing hair cells by treating explanted basilar papilla with aminoglycoside antibiotics, supporting cells differentiated into hair cells (either after proliferating or directly via transdifferentiation), and *Bmp4* was also expressed in such regenerated hair cells (Lewis et al., 2018). Application of Bmp4 with the ototoxic antibiotic blocked hair cell regeneration by preventing supporting cells from proliferating and upregulating *Atoh1* (Lewis et al., 2018). Conversely, application of the extracellular Bmp4/2/7 antagonist Noggin (Zimmerman et al., 1996) together with the ototoxic antibiotic led to the formation of significantly more hair cells per unit area than in control cultures (Lewis et al., 2018). Taken together, these results suggest that in the mature auditory epithelium, Bmp4 secreted from existing hair cells prevents supporting cells from forming supernumerary hair cells; after hair-cell death, Bmp4 is lost and this inhibition is relieved, allowing hair cell regeneration (Lewis et al., 2018).

The regeneration of supernumerary hair cells in the mature chicken auditory epithelium after inhibiting Bmp signalling with Noggin (Lewis et al., 2018) was reminiscent of the formation of supernumerary ampullary organs after inhibiting Bmp signalling with DMH1, prior to the onset of ampullary organ development. Indeed, we also note the action of Bmps as inhibitors in reaction-diffusion (Turing) systems (see Green and Sharpe, 2015) that result in the periodic spacing of hair follicles (Mou et al., 2006), feather primordia (Jung et al., 1998; Noramly and

Morgan, 1998; Jiang et al., 1999; Michon et al., 2008) and potentially also denticles in shark skin (Cooper et al., 2018). Sterlet *Bmp4* was expressed in the regions where ampullary organs and neuromasts are forming on the head (and more strongly in the migrating lateral line primordia on the trunk), but only weakly and transiently in developing ampullary organs and neuromasts themselves. This could be consistent with a role for Bmp4 in promoting formation of the prosensory domain within which the sensory organs develop, as seen for inner ear sensory patches (Chang et al., 2008; Ohyama et al., 2010). Its subsequent downregulation in developing lateral line organs in sterlet differs from the expression of chicken *Bmp4* in the vestibular cristae (*Bmp4*-positive supporting cells; Kamaid et al., 2010) and auditory basilar papilla (*Bmp4*-positive hair cells; Lewis et al., 2018). However, *Bmp5* is expressed in mature ampullary organs and neuromasts and additional as-yet unidentified Bmp ligand genes may also be expressed, given the more extensive pattern of pSMAD1/5/9 immunoreactivity. Overall, the precise mechanism by which Bmp signalling normally prevents supernumerary and ectopic ampullary organ formation remains to be established, but the data from the chicken auditory epithelium (Lewis et al., 2018) and reaction-diffusion systems patterning other skin structures (see Green and Sharpe, 2015) provide potential parallels for future investigation.

We recently reported that the transcription factor gene *Foxg1* is expressed in paddlefish and sterlet in the central region of sensory ridges where neuromasts form (Minařík et al., 2024a), and that targeting *Foxg1* for CRISPR/Cas9-mediated led to ampullary organs forming within neuromast lines (preprint, Minařík et al., 2024b). Here, we found that Bmp signalling is required to prevent supernumerary ampullary organ formation within ampullary organ fields, including ectopic ampullary organs within the small dorsalmost fields, although neuromast lines developed normally (apart from the ectopic offshoot of the supraorbital line; see next section). Although these phenotypes are distinct, a common theme emerges, namely the active repression of ampullary organ formation during normal development: within neuromast lines by Foxg1, and within ampullary organ fields by Bmp signalling. Taken together, this suggests that lateral line primordia are 'poised' to form ampullary organs (indeed potentially that ampullary organs are the 'default' fate for lateral line primordia in electroreceptive species; preprint, Minařík et al., 2024b), and this must be controlled to ensure that ampullary organs develop in the 'correct' number and location.

Bmp signalling activity prevents ectopic secondary neuromast formation in the supraorbital neuromast line

An ectopic offshoot of the supraorbital neuromast line also developed by stage 45 in a majority of larvae that had been treated with DMH1 to block Bmp signalling for 20 hours from hatching (stages 36-38). Intriguingly, pSMAD1/5/9 immunoreactivity (a proxy for Bmp signalling activity)

was particularly prominent within lateral line nerves from stages 36-40, including the supraorbital nerve (nerve immunoreactivity had almost disappeared by stage 42), and was also prominent in the supraorbital region at later stages. Afferent innervation is not required for the formation of neuromasts deposited by lateral line primordia in zebrafish (Andermann et al., 2002; Grant et al., 2005; López-Schier and Hudspeth, 2005). However, the post-embryonic budding of neuromasts to form short rows ("stitches") of additional neuromasts depends on Wnt signalling from afferent axons: this promotes cell proliferation within the neuromast, which is required for the budding process (Wada et al., 2013; Wada and Kawakami, 2015). We speculate that Bmp signalling in the lateral line nerve may act to inhibit this process during embryogenesis, thus preventing precocious budding of primary neuromasts. This hypothesis remains to be tested.

Conclusion

Overall, we have identified dual opposing roles for Bmp signalling during the development of electrosensory ampullary organs in the sterlet. CRISPR/Cas9-mediated mutagenesis in G0-injected embryos showed that *Bmp5*, which is expressed within ampullary organ primordia (and later in mature ampullary organs and neuromasts), is required for ampullary organ formation. Conversely, global inhibition of type I Bmp receptors via DMH1 treatment at stages just prior to the onset of ampullary organ development, revealed that Bmp signalling is required to prevent supernumerary and ectopic ampullary organs from forming. Future work will be required to understand the respective mechanisms involved.

Materials and Methods

Collection, staging and fixation of sterlet embryos and larvae

Fertilised sterlet (*Acipenser ruthenus*) eggs were obtained during the annual spawning season at the Research Institute of Fish Culture and Hydrobiology (RIFCH), Faculty of Fisheries and Protection of Waters, University of South Bohemia in České Budějovice (Vodňany, Czech Republic). Comprehensive information about sterlet husbandry, *in vitro* fertilisation and the rearing of embryos and yolk-sac larvae is provided by Stundl et al. (2022). A mix of sperm from three different males was used for each fertilisation, so each batch comprised siblings and half-siblings. At desired stages (Dettlaff et al., 1993), embryos/larvae were euthanised by anaesthetic overdose using MS-222 (Sigma-Aldrich) before fixation in modified Carnoy's fixative (6 volumes 100% ethanol: 3 volumes 37% formaldehyde: 1 volume glacial acetic acid) for 3 hours at room temperature and graded into ethanol for storage at -20°C.

All experimental procedures were approved by the Animal Research Committee of the Faculty of Fisheries and Protection of Waters in Vodňany, University of South Bohemia in

České Budějovice, Czech Republic, and by the Ministry of Agriculture of the Czech Republic (reference number: MSMT-12550/2016-3). Experimental fish were maintained according to the principles of the European Union (EU) Harmonized Animal Welfare Act of the Czech Republic, and Principles of Laboratory Animal Care and National Laws 246/1992 “Animal Welfare” on the protection of animals.

Gene cloning, *in situ* hybridisation and immunohistochemistry

Total RNA was extracted from the heads of stage 45 sterlet larvae using Trizol (Invitrogen, Thermo Fisher Scientific), treated with DNAse using the Ambion Turbo DNA-free kit (Invitrogen, Thermo Fisher Scientific) and cDNA synthesised using the High-Capacity cDNA Reverse Transcription Kit (Applied Biosystems), following the manufacturers' instructions. Genes were selected from the late-larval paddlefish (*Polyodon spathula*) lateral line organ-enriched gene-set (National Center for Biotechnology Information [NCBI] Gene Expression Omnibus accession code GSE92470; Modrell et al., 2017a) or via a candidate approach. The relevant paddlefish transcriptome sequence was used in a command-line search of a Basic Local Alignment Search Tool (BLAST) database generated from our sterlet transcriptome assemblies (from pooled late-larval sterlet heads at stages 40-45; Minařík et al., 2024a), which are available at DDBJ/EMBL/GenBank under the accessions GKLU00000000 and GKEF01000000. Sterlet sequence identity was confirmed using NCBI BLAST (https://blast.ncbi.nlm.nih.gov/Blast.cgi; McGinnis and Madden, 2004). PCR primers (Supplementary Table S4) were designed using Primer3Plus (Untergasser et al., 2012), which is also integrated into Benchling’s Editor program (https://benchling.com), and used under standard PCR conditions to amplify cDNA fragments from sterlet cDNA. These were cloned into Qiagen's pDrive cloning vector using the Qiagen PCR Cloning Kit (Qiagen) and clones verified by sequencing (Department of Biochemistry Sequencing Facility, University of Cambridge). Sequence identity was confirmed using NCBI BLAST. Alternatively, sterlet transcriptome data were used to design synthetic gene fragments with added M13 forward and reverse primer adaptors, which were purchased from Twist Bioscience.

Chromosome-level genome assemblies for sterlet (Du et al., 2020) and the 2022 reference genome, NCBI Refseq assembly GCF_902713425.1/) had not been published when these sterlet riboprobe template sequences were designed. Both ohnologs (gene paralogs resulting from whole-genome duplication) for all genes described here have been retained from the independent whole-genome duplication in the sterlet lineage (Du et al., 2020). Supplementary Table S4 includes each riboprobe’s percentage match with each ohnolog, obtained by using NCBI BLAST to perform a nucleotide BLAST search against the respective genome assemblies. The percentage match with the "targeted" ohnolog ranged from 99.2-100%. The percentage match with the second ohnolog ranged from 90.0-100%,

suggesting that our riboprobes most likely also target transcripts from the second ohnolog. GenBank accession numbers for the top match for each riboprobe, and the nucleotide ranges targeted, are given in Supplementary Table S4.

Digoxigenin-labelled riboprobes were synthesised as previously described (Minařík et al., 2024a). Wholemount *in situ* hybridisation (ISH) was performed as described in Modrell et al. (2011a). Wholemount immunostaining was performed as described in Metscher and Müller (2011). Primary antibodies (anti-Sox2: Abcam ab92494, rabbit monoclonal, 1:200; anti-Phospho-SMAD1/5/9: Cell Signalling Technology D5B10, rabbit monoclonal, 1:100) were applied in blocking solution for 24 hours at 4°C, as was the secondary antibody (horseradish peroxidase-conjugated goat anti-rabbit IgG: Jackson ImmunoResearch, 1:500). The metallographic peroxidase substrate EnzMet kit (Nanoprobes 6010) was used for the colour reaction, following the manufacturer's instructions. For both ISH and immunostaining, at least three embryos/larvae were used per stage.

CRISPR guide RNA design and synthesis

Prior to the publication of chromosome-level sterlet genomes (Du et al., 2020 and the 2022 NCBI RefSeq assembly GCF_902713425.1), *Bmp5* was identified using NCBI BLAST to search draft genomic sequence data (M.H., unpublished). Exons were confirmed by comparison with spotted gar (*Lepisosteus oculatus*) using Ensembl (Cunningham et al., 2022). NCBI BLASTX (https://blast.ncbi.nlm.nih.gov/Blast.cgi; McGinnis and Madden, 2004) was used to identify conserved domains. Four CRISPR single guide RNAs (sgRNAs) were designed using the CRISPR Guide RNA Design Tool from Benchling (https://benchling.com) to target a 450-base region within exon 1 that encodes part of the TGFβ propeptide domain (Table 1; Supplementary Figure S5A). The previously published guides against *tyrosinase* were designed as described in Minařík et al. (2024b, preprint).

Plasmid pX335-U6-Chimeric_BB-CBh-hSpCas9n(D10A) (Addgene, plasmid #42335; Cong et al., 2013) was used to synthesize DNA templates containing the single guide (sg)RNA scaffold, which was amplified using the same reverse primer for all reactions (AAAAAAGCACCGACTCGGTGCC) and a specific forward primer for each sgRNA. The forward primer had an overhang containing the T7 promoter and the 20-nucleotide sgRNA target sequence: GATCACTAATACGACTCACTATA(20N)GTTTTAGAGCTAGAAAT, where the T7 promoter is underlined and "(20N)" represents the target sequence specific to each sgRNA (Table 1). Where the first nucleotide of the target sequence was G, this completed the T7 promoter (and became the first base of the sgRNA). Where the target sequence did not start with G, an additional G was added before the target sequence to complete the T7 promoter and ensure efficient transcription. Alternatively, chemically modified synthetic gRNAs were purchased from Synthego (CRISPRevolution sgRNA EZ Kit).

957

958 **Embryo injections and genotyping**

959 A detailed description of sterlet embryo injection is provided in Minařík et al. (2024b, preprint).
960 Briefly, 2400 ng Cas9 protein with NLS (PNA Bio CP01) were combined with 1200 ng of
961 sgRNA in 4.5 µl nuclease-free water on the day of injection and left at room temperature for
962 10 minutes to form ribonucleoprotein complexes, then kept on ice. For sgRNA multiplexing,
963 different Cas9-sgRNA complexes were combined 1:1 and 0.5 µl 10% 10,000 MW rhodamine
964 dextran (Invitrogen) added to a final volume of 5 µl. One- or 2-cell stage embryos were injected
965 with approximately 20 nl of the injection mixture (manually or using an Eppendorf FemtoJet
966 4x microinjector) and maintained at 20°C until the 64-cell stage, then transferred to 16°C.
967 Upon reaching stage 45, they were euthanised by MS-222 overdose, fixed with modified
968 Carnoy's fixative and dehydrated into ethanol as described above. Prior to ISH, fixed crispants
969 were cut in half and the tails set aside for genotyping. DNA was extracted from crispant tails
970 using the PCRBIO Rapid Extract PCR Kit (PCR Biosystems) and the target region amplified
971 using HS Taq Mix Red (PCR Biosystems) following the manufacturer's instructions.
972 Genotyping primers (Supplementary Table S1) were designed using Benchling's Editor
973 program (https://benchling.com) to flank the sgRNA target region with a buffer of at least 150
974 bp. PCR products were subjected to agarose gel electrophoresis, extracted using the MinElute
975 Gel Extraction Kit (Qiagen) according to the manufacturer's protocol and sequenced by
976 Genewiz (Azenta Life Sciences). The resulting Sanger trace files were uploaded for analysis
977 by Synthego's Inference of CRISPR Edits (ICE) tool (Conant et al., 2022).

978

979 **Small-molecule inhibition of Bmp signalling**

980 Stage 36 (post-hatching) yolksac larvae were incubated for 20 hours in 50 µM DMH1 (Cayman
981 Chemical) in 1% dimethyl sulfoxide (DMSO) or in 1% DMSO as a control. After treatment, the
982 larvae were rinsed thoroughly, transferred to new water and left to develop until approximately
983 stage 45, then euthanised by MS-222 overdose and fixed in modified Carnoy's solution as
984 described above.

985

986 **Image capture and processing**

987 Embryos/larvae were imaged using a Leica MZFLIII dissecting microscope fitted either with a
988 QImaging MicroPublisher 5.0 RTV camera using QCapture Pro 7.0 software (QImaging) or a
989 MicroPublisher 6 color CCD camera (Teledyne Photometrics) using Ocular software
990 (Teledyne Photometrics). In most cases, focus stacking was performed using Helicon Focus
991 software (Helicon Soft Limited) on image-stacks collected by manually focusing through the
992 sample. Images were processed using Adobe Photoshop (Adobe Systems Inc.).

993

994 **Statistical analysis**

995 Initial data analysis was performed using Microsoft Excel. GraphPad Prism 10 (GraphPad
996 Software, La Jolla, CA, USA) was used to compare datasets using a two-tailed Mann-Whitney
997 (Wilcoxon rank sum) test and to generate scatter plots showing the median and interquartile
998 range. The raw data are provided in Supplementary Tables S2 and S3.
999

1000 **Data availability statement**

1001 The publication and associated supplementary figures include representative example images
1002 of embryos/larvae from each experiment. Additional data underlying this publication consist of
1003 further images of these and other embryos/larvae from each experiment. Public sharing of
1004 these images is not cost-efficient, but they are available from the corresponding author upon
1005 reasonable request. Previously published sterlet transcriptome assemblies (from pooled stage
1006 40-45 sterlet heads; Minařík et al., 2024a) are available at DDBJ/EMBL/GenBank under the
1007 accessions GKLU00000000 (https://www.ncbi.nlm.nih.gov/nuccore/GKLU00000000) and
1008 GKEF01000000 (https://www.ncbi.nlm.nih.gov/nuccore/GKEF00000000.1). Previously
1009 published paddlefish RNA-seq data (from pooled paddlefish opercula and fin tissue at stage
1010 46; Modrell et al., 2017a) are available via the NCBI Gene Expression Omnibus (GEO)
1011 database (https://www.ncbi.nlm.nih.gov/geo/) under accession code GSE92470.
1012

1013 **Ethics statement**

1014 Sterlet animal work was reviewed and approved by The Animal Research Committee of
1015 Research Institute of Fish Culture and Hydrobiology, Faculty of Fisheries and Protection of
1016 Waters, University of South Bohemia in České Budějovice, Vodňany, Czech Republic and
1017 Ministry of Agriculture of the Czech Republic (MSMT-12550/2016-3). Experimental fish were
1018 maintained according to the principles of the European Union (EU) Harmonized Animal
1019 Welfare Act of the Czech Republic, and Principles of Laboratory Animal Care and National
1020 Laws 246/1992 “Animal Welfare” on the protection of animals.
1021

1022 **Author contributions**

1023 CB conceived and designed the project, provided guidance and helped to write the manuscript
1024 together with AC. AC led the project, performed most of the experiments and statistical
1025 analyses, prepared all of the manuscript figures, and wrote the first draft of the manuscript.
1026 MM and RF performed some experiments. MV provided essential support for the experiments.
1027 MH contributed draft genome sequence data. MP and DG were instrumental in enabling all
1028 work with sterlet embryos. All authors read and commented on the manuscript.
1029
1030

Funding

This work was supported by the Anatomical Society and by the Biotechnology and Biological Sciences Research Council (BBSRC: grant BB/P001947/1 to CB). AC was supported by a PhD research studentship from the Anatomical Society with additional funding from the Cambridge Philosophical Society. Additional support for MM was provided by the Cambridge Isaac Newton Trust (grant 20.07[c] to CB) and by the School of the Biological Sciences, University of Cambridge. The work of RF, MV and MP was supported by the Ministry of Education, Youth and Sports of the Czech Republic, projects CENAKVA (LM2018099), Biodiversity (CZ.02.1.01/0.0/0.0/16_025/0007370) and Czech Science Foundation (22-31141J).

Acknowledgments

Thanks to Marek Rodina and Martin Kahanec for their help with sterlet spawns.

Conflict of Interest: The authors declare that the research was conducted in the absence of any commercial or financial relationships that could be construed as a potential conflict of interest.

References

Andermann, P., Ungos, J., Raible, D.W., 2002. Neurogenin1 defines zebrafish cranial sensory ganglia precursors. Dev. Biol. 251, 45-58.

Bai, H., Jiang, L., Wang, X., Gao, X., Bing, J., Xi, C., Wang, W., Zhang, M., Zhang, X., Han, Z., Xu, J., Zeng, S., 2019. Transcriptomic analysis of mouse cochleae suffering from gentamicin damage reveals the signalling pathways involved in hair cell regeneration. Sci. Rep. 9, 10494.

Baker, C.V.H., 2019. The development and evolution of lateral line electroreceptors: insights from comparative molecular approaches., in: B.A. Carlson, J.A. Sisneros, A.N. Popper, R.R. Fay (Eds.), Electroreception: Fundamental Insights from Comparative Approaches. Springer, Cham, pp. 25-62.

Baker, C.V.H., Modrell, M.S., 2018. Insights into electroreceptor development and evolution from molecular comparisons with hair cells. Integr. Comp. Biol. 58, 329-340.

1068 Baker, C.V.H., Modrell, M.S., Gillis, J.A., 2013. The evolution and development of vertebrate
1069 lateral line electroreceptors. J. Exp. Biol. 216, 2515-2522.
1070 Bodznick, D., Montgomery, J.C., 2005. The physiology of low-frequency electrosensory
1071 systems, in: T.H. Bullock, C.D. Hopkins, A.N. Popper, R.R. Fay (Eds.), Electroreception.
1072 Springer, New York, pp. 132-153.
1073 Bullock, T.H., Bodznick, D.A., Northcutt, R.G., 1983. The phylogenetic distribution of
1074 electroreception: evidence for convergent evolution of a primitive vertebrate sense
1075 modality. Brain Res. Rev. 287, 25-46.
1076 Camacho, S., Ostos, M.D.V., Llorente, J.I., Sanz, A., García, M., Domezain, A., Carmona, R.,
1077 2007. Structural characteristics and development of ampullary organs in *Acipenser*
1078 *naccarii*. Anat. Rec. 290, 1178-1189.
1079 Cernuda-Cernuda, R., García-Fernández, J.M., 1996. Structural diversity of the ordinary and
1080 specialized lateral line organs. Microsc. Res. Tech. 34, 302-312.
1081 Chagnaud, B.P., Wilkens, L.A., Hofmann, M., 2021. The ampullary electrosensory system – a
1082 paddlefish case study, in: B. Fritzsch (Ed.), The Senses: A Comprehensive Reference.
1083 Elsevier, pp. 215-227.
1084 Chang, W., Lin, Z., Kulessa, H., Hebert, J., Hogan, B.L., Wu, D.K., 2008. *Bmp4* is essential
1085 for the formation of the vestibular apparatus that detects angular head movements. PLoS
1086 Genet. 4, e1000050.
1087 Chitnis, A.B., 2021. Development of the zebrafish posterior lateral line system, in: B. Fritzsch
1088 (Ed.), The Senses: A Comprehensive Reference. Elsevier, pp. 66-84.
1089 Conant, D., Hsiau, T., Rossi, N., Oki, J., Maures, T., Waite, K., Yang, J., Joshi, S., Kelso, R.,
1090 Holden, K., Enzmann, B.L., Stoner, R., 2022. Inference of CRISPR edits from Sanger
1091 trace data. CRISPR J. 5, 123-130.
1092 Cong, L., Ran, F.A., Cox, D., Lin, S., Barretto, R., Habib, N., Hsu, P.D., Wu, X., Jiang, W.,
1093 Marraffini, L.A., Zhang, F., 2013. Multiplex genome engineering using CRISPR/Cas
1094 systems. Science 339, 819-823.
1095 Cooper, R.L., Thiery, A.P., Fletcher, A.G., Delbarre, D.J., Rasch, L.J., Fraser, G.J., 2018. An
1096 ancient Turing-like patterning mechanism regulates skin denticle development in sharks.
1097 Sci. Adv. 4, eaau5484.
1098 Crampton, W.G.R., 2019. Electroreception, electrogenesis and electric signal evolution. J.
1099 Fish Biol. 95, 92-134.
1100 Cross, E.E., Thomason, R.T., Martinez, M., Hopkins, C.R., Hong, C.C., Bader, D.M., 2011.
1101 Application of small organic molecules reveals cooperative TGFβ and BMP regulation of
1102 mesothelial cell behaviors. ACS Chem. Biol. 6, 952-961.
1103 Cunningham, F., Allen, J.E., Allen, J., Alvarez-Jarreta, J., Amode, M.R., Armean, I.M., Austine-
1104 Orimoloye, O., Azov, A.G., Barnes, I., Bennett, R., Berry, A., Bhai, J., Bignell, A., Billis,

K., Boddu, S., Brooks, L., Charkhchi, M., Cummins, C., Da Rin Fioretto, L., Davidson, C., Dodiya, K., Donaldson, S., El Houdaigui, B., El Naboulsi, T., Fatima, R., Giron, C.G., Genez, T., Martinez, J.G., Guijarro-Clarke, C., Gymer, A., Hardy, M., Hollis, Z., Hourlier, T., Hunt, T., Juettemann, T., Kaikala, V., Kay, M., Lavidas, I., Le, T., Lemos, D., Marugán, J.C., Mohanan, S., Mushtaq, A., Naven, M., Ogeh, D.N., Parker, A., Parton, A., Perry, M., Piližota, I., Prosovetskaia, I., Sakthivel, M.P., Salam, A.I.A., Schmitt, B.M., Schuilenburg, H., Sheppard, D., Pérez-Silva, J.G., Stark, W., Steed, E., Sutinen, K., Sukumaran, R., Sumathipala, D., Suner, M.M., Szpak, M., Thormann, A., Tricomi, F.F., Urbina-Gómez, D., Veidenberg, A., Walsh, T.A., Walts, B., Willhoft, N., Winterbottom, A., Wass, E., Chakiachvili, M., Flint, B., Frankish, A., Giorgetti, S., Haggerty, L., Hunt, S.E., IIsley, G.R., Loveland, J.E., Martin, F.J., Moore, B., Mudge, J.M., Muffato, M., Perry, E., Ruffier, M., Tate, J., Thybert, D., Trevanion, S.J., Dyer, S., Harrison, P.W., Howe, K.L., Yates, A.D., Zerbino, D.R., Flicek, P., 2022. Ensembl 2022. Nucleic Acids Res. 50, D988-D995.

Dettlaff, T.A., Ginsburg, A.S., Schmalhausen, O.I., 1993. Sturgeon Fishes: Developmental Biology and Aquaculture. Springer-Verlag, Berlin.

Du, K., Stöck, M., Kneitz, S., Klopp, C., Woltering, J.M., Adolfi, M.C., Feron, R., Prokopov, D., Makunin, A., Kichigin, I., Schmidt, C., Fischer, P., Kuhl, H., Wuertz, S., Gessner, J., Kloas, W., Cabau, C., Iampietro, C., Parrinello, H., Tomlinson, C., Journot, L., Postlethwait, J.H., Braasch, I., Trifonov, V., Warren, W.C., Meyer, A., Guiguen, Y., Schartl, M., 2020. The sterlet sturgeon genome sequence and the mechanisms of segmental rediploidization. Nat. Ecol. Evol. 4, 841-852.

Fan, C., Zou, S., Wang, J., Zhang, B., Song, J., 2016. Neomycin damage and regeneration of hair cells in both mechanoreceptor and electroreceptor lateral line organs of the larval Siberian sturgeon (*Acipenser baerii*). J. Comp. Neurol. 524, 1443-1456.

Gibbs, M.A., Northcutt, R.G., 2004. Development of the lateral line system in the shovelnose sturgeon. Brain Behav. Evol. 64, 70-84.

Gilmour, D., Knaut, H., Maischein, H.M., Nüsslein-Volhard, C., 2004. Towing of sensory axons by their migrating target cells *in vivo*. Nat. Neurosci. 7, 491-492.

Gilmour, D.T., Maischein, H.M., Nusslein-Volhard, C., 2002. Migration and function of a glial subtype in the vertebrate peripheral nervous system. Neuron 34, 577-588.

Grant, K.A., Raible, D.W., Piotrowski, T., 2005. Regulation of latent sensory hair cell precursors by glia in the zebrafish lateral line. Neuron 45, 69-80.

Green, J.B.A., Sharpe, J., 2015. Positional information and reaction-diffusion: two big ideas in developmental biology combine. Development 142, 1203-1211.

1140 Guo, X., Zhang, T., Hu, Z., Zhang, Y., Shi, Z., Wang, Q., Cui, Y., Wang, F., Zhao, H., Chen,
1141 Y., 2014. Efficient RNA/Cas9-mediated genome editing in *Xenopus tropicalis*.
1142 Development 141, 707-714.
1143 Hao, J., Ho, J.N., Lewis, J.A., Karim, K.A., Daniels, R.N., Gentry, P.R., Hopkins, C.R.,
1144 Lindsley, C.W., Hong, C.C., 2010. *In vivo* structure-activity relationship study of
1145 dorsomorphin analogues identifies selective VEGF and BMP inhibitors. ACS Chem. Biol.
1146 5, 245-253.
1147 Heller, I.S., Guenther, C.A., Meireles, A.M., Talbot, W.S., Kingsley, D.M., 2022.
1148 Characterization of mouse *Bmp5* regulatory injury element in zebrafish wound models.
1149 Bone 155, 116263.
1150 Hernández, P.P., Olivari, F.A., Sarrazin, A.F., Sandoval, P.C., Allende, M.L., 2007.
1151 Regeneration in zebrafish lateral line neuromasts: expression of the neural progenitor
1152 cell marker sox2 and proliferation-dependent and-independent mechanisms of hair cell
1153 renewal. Dev. Neurobiol. 67, 637-654.
1154 Jiang, L., Romero-Carvajal, A., Haug, J.S., Seidel, C.W., Piotrowski, T., 2014. Gene-
1155 expression analysis of hair cell regeneration in the zebrafish lateral line. Proc. Natl. Acad.
1156 Sci. U.S.A. 111, E1383-92.
1157 Jiang, T.-X., Jung, H.-S., Widelitz, R.B., Chuong, C.-M., 1999. Self-organization of periodic
1158 patterns by dissociated feather mesenchymal cells and the regulation of size, number
1159 and spacing of primordia. Development 126, 4997-5009.
1160 Jørgensen, J.M., 2005. Morphology of electroreceptive sensory organs, in: T.H. Bullock, C.D.
1161 Hopkins, A.N. Popper, R.R. Fay (Eds.), Electroreception. Springer, New York, pp. 47-
1162 67.
1163 Jørgensen, J.M., 2011. Morphology of electroreceptive sensory organs, in: A.P. Farrell (Ed.),
1164 Encyclopedia of Fish Physiology: From Genome to Environment. Academic Press, San
1165 Diego, pp. 350-358.
1166 Josberger, E.E., Hassanzadeh, P., Deng, Y., Sohn, J., Rego, M.J., Amemiya, C.T., Rolandi,
1167 M., 2016. Proton conductivity in ampullae of Lorenzini jelly. Sci. Adv. 2, e1600112.
1168 Jung, H.-S., Francis-West, P.H., Widelitz, R.B., Jiang, T.-X., Ting-Berreth, S., Tickle, C.,
1169 Wolpert, L., Chuong, C.M., 1998. Local inhibitory action of BMPs and their relationships
1170 with activators in feather formation: implications for periodic patterning. Dev. Biol. 196,
1171 11-23.
1172 Kamaid, A., Neves, J., Giráldez, F., 2010. *Id* gene regulation and function in the prosensory
1173 domains of the chicken inner ear: a link between Bmp signaling and *Atoh1*. J. Neurosci.
1174 30, 11426-11434.
1175 Leitch, D.B., Julius, D., 2019. Electrosensory transduction: comparisons across structure,
1176 afferent response properties, and cellular physiology., in: B.A. Carlson, J.A. Sisneros,

A.N. Popper, R.R. Fay (Eds.), Electroreception: Fundamental Insights from Comparative Approaches. Springer, Cham, pp. 63-90.

Lewis, R.M., Keller, J.J., Wan, L., Stone, J.S., 2018. Bone morphogenetic protein 4 antagonizes hair cell regeneration in the avian auditory epithelium. Hear. Res. 364, 1-11.

Li, H., Corrales, C.E., Wang, Z., Zhao, Y., Wang, Y., Liu, H., Heller, S., 2005. BMP4 signaling is involved in the generation of inner ear sensory epithelia. BMC Dev. Biol. 5, 16.

López-Schier, H., Hudspeth, A.J., 2005. Supernumerary neuromasts in the posterior lateral line of zebrafish lacking peripheral glia. Proc. Natl. Acad. Sci. U.S.A. 102, 1496-1501.

Ludwig, A., Belfiore, N.M., Pitra, C., Svirsky, V., Jenneckens, I., 2001. Genome duplication events and functional reduction of ploidy levels in sturgeon (*Acipenser*, *Huso* and *Scaphirhynchus*). Genetics 158, 1203-1215.

Lush, M.E., Diaz, D.C., Koenecke, N., Baek, S., Boldt, H., St Peter, M.K., Gaitan-Escudero, T., Romero-Carvajal, A., Busch-Nentwich, E.M., Perera, A.G., Hall, K.E., Peak, A., Haug, J.S., Piotrowski, T., 2019. scRNA-Seq reveals distinct stem cell populations that drive hair cell regeneration after loss of Fgf and Notch signaling. eLife 8, e44431.

Lush, M.E., Piotrowski, T., 2014. Sensory hair cell regeneration in the zebrafish lateral line. Dev. Dyn. 243, 1187-1202.

McGinnis, S., Madden, T.L., 2004. BLAST: at the core of a powerful and diverse set of sequence analysis tools. Nucleic Acids Res. 32, W20-5.

McGraw, H.F., Drerup, C.M., Nicolson, T., Nechiporuk, A.V., 2017. The molecular and cellular mechanisms of zebrafish lateral line development, in: K.S. Cramer, A.B. Coffin, R.R. Fay, A.N. Popper (Eds.), Auditory Development and Plasticity. New York, pp. 49-73.

Metcalfe, W.K., 1985. Sensory neuron growth cones comigrate with posterior lateral line primordial cells in zebrafish. J. Comp. Neurol. 238, 218-224.

Metscher, B.D., Müller, G.B., 2011. MicroCT for molecular imaging: quantitative visualization of complete three-dimensional distributions of gene products in embryonic limbs. Dev. Dyn. 240, 2301-2308.

Michon, F., Forest, L., Collomb, E., Demongeot, J., Dhouailly, D., 2008. BMP2 and BMP7 play antagonistic roles in feather induction. Development 135, 2797-2805.

Minařík, M., Modrell, M.S., Gillis, J.A., Campbell, A.S., Fuller, I., Lyne, R., Micklem, G., Gela, D., Pšenička, M., Baker, C.V.H., 2024a. Identification of multiple transcription factor genes potentially involved in the development of electrosensory versus mechanosensory lateral line organs. Front. Cell Dev. Biol. 12, 1327924.

Minařík, M., Campbell, A.S., Franěk, R., Vazačová, M., Havelka, M., Gela, D., Pšenička, M., Baker, C.V.H., 2024b. Atoh1 is required for the formation of lateral line electroreceptors

and hair cells, whereas Foxg1 represses an electrosensory fate. bioRxiv doi: https://doi.org/10.1101/2023.04.15.537030.

Modrell, M.S., Bemis, W.E., Northcutt, R.G., Davis, M.C., Baker, C.V.H., 2011a. Electrosensory ampullary organs are derived from lateral line placodes in bony fishes. Nat. Commun. 2, 496.

Modrell, M.S., Buckley, D., Baker, C.V.H., 2011b. Molecular analysis of neurogenic placode development in a basal ray-finned fish. genesis 49, 278-294.

Modrell, M.S., Lyne, M., Carr, A.R., Zakon, H.H., Buckley, D., Campbell, A.S., Davis, M.C., Micklem, G., Baker, C.V.H., 2017a. Insights into electrosensory organ development, physiology and evolution from a lateral line-enriched transcriptome. eLife 6, e24197.

Modrell, M.S., Tidswell, O.R.A., Baker, C.V.H., 2017b. Notch and Fgf signaling during electrosensory versus mechanosensory lateral line organ development in a non-teleost ray-finned fish. Dev. Biol. 431, 48-58.

Mogdans, J., 2021. Physiology of the peripheral lateral line system, in: B. Fritzsch (Ed.), The Senses: A Comprehensive Reference. Elsevier, pp. 143-162.

Montgomery, J., Bleckmann, H., Coombs, S., 2014. Sensory ecology and neuroethology of the lateral line, in: S.C. Coombs, H. Bleckmann, R.R. Fay, A.N. Popper (Eds.), The Lateral Line System. Springer, New York, pp. 121-150.

Morsli, H., Choo, D., Ryan, A., Johnson, R., Wu, D.K., 1998. Development of the mouse inner ear and origin of its sensory organs. J. Neurosci. 18, 3327-3335.

Mou, C., Jackson, B., Schneider, P., Overbeek, P.A., Headon, D.J., 2006. Generation of the primary hair follicle pattern. Proc. Natl. Acad. Sci. U.S.A. 103, 9075-9080.

Mowbray, C., Hammerschmidt, M., Whitfield, T.T., 2001. Expression of BMP signalling pathway members in the developing zebrafish inner ear and lateral line. Mech. Dev. 108, 179-184.

Nikaido, M., Acedo, J.N., Hatta, K., Piotrowski, T., 2017. Retinoic acid is required and Fgf, Wnt, and Bmp signaling inhibit posterior lateral line placode induction in zebrafish. Dev. Biol. 431, 215-225.

Noramly, S., Morgan, B.A., 1998. BMPs mediate lateral inhibition at successive stages in feather tract development. Development 125, 3775-3787.

Northcutt, R.G., 1997. Evolution of gnathostome lateral line ontogenies. Brain Behav. Evol. 50, 25-37.

Northcutt, R.G., 2005. Ontogeny of electroreceptors and their neural circuitry, in: T.H. Bullock, C.D. Hopkins, A.N. Popper, R.R. Fay (Eds.), Electroreception. Springer, New York, pp. 112-131.

Ohyama, T., Basch, M.L., Mishina, Y., Lyons, K.M., Segil, N., Groves, A.K., 2010. BMP signaling is necessary for patterning the sensory and nonsensory regions of the developing mammalian cochlea. J. Neurosci. 30, 15044-15051.

Pickett, S.B., Raible, D.W., 2019. Water waves to sound waves: using zebrafish to explore hair cell biology. J. Assoc. Res. Otolaryngol. 20, 1-19.

Piotrowski, T., Baker, C.V.H., 2014. The development of lateral line placodes: Taking a broader view. Dev. Biol. 389, 68-81.

Pujades, C., Kamaid, A., Alsina, B., Giraldez, F., 2006. BMP-signaling regulates the generation of hair-cells. Dev. Biol. 292, 55-67.

Rabinowitz, R., Offen, D., 2021. Single-base resolution: increasing the specificity of the CRISPR-Cas system in gene editing. Mol. Ther. 29, 937-948.

Russell, D.F., Zhang, W., Warnock, T.C., Neiman, L.L., 2022. Lectin binding and gel secretion within Lorenzinian electroreceptors of *Polyodon*. PLoS One 17, e0276854.

Schmierer, B., Hill, C.S., 2007. TGFbeta-SMAD signal transduction: molecular specificity and functional flexibility. Nat Rev Mol Cell Biol 8, 970-982.

Stundl, J., Soukup, V., Franěk, R., Pospisilova, A., Psutkova, V., Pšenička, M., Cerny, R., Bronner, M.E., Medeiros, D.M., Jandzik, D., 2022. Efficient CRISPR mutagenesis in sturgeon demonstrates its utility in large, slow-maturing vertebrates. Front. Cell Dev. Biol. 10, 750833.

Thisse, B., Thisse, C., 2004. Fast release clones: a high throughput expression analysis. ZFIN Direct Data Submission (http://zfin.org).

Tong, X., Zhu, C., Liu, L., Huang, M., Xu, J., Chen, X., Zou, J., 2022. Role of Sostdc1 in skeletal biology and cancer. Front. Physiol. 13, 1029646.

Undurraga, C.A., Gou, Y., Sandoval, P.C., Nuñez, V.A., Allende, M.L., Riley, B.B., Hernández, P.P., Sarrazin, A.F., 2019. Sox2 and Sox3 are essential for development and regeneration of the zebrafish lateral line. bioRxiv 856088; doi: https://doi.org/10.1101/856088.

Untergasser, A., Cutcutache, I., Koressaar, T., Ye, J., Faircloth, B.C., Remm, M., Rozen, S.G., 2012. Primer3 - new capabilities and interfaces. Nucl. Acids Res. 40, e115.

Uribe-Salazar, J.M., Kaya, G., Sekar, A., Weyenberg, K., Ingamells, C., Dennis, M.Y., 2022. Evaluation of CRISPR gene-editing tools in zebrafish. BMC Genomics 23, 12.

Vonica, A., Bhat, N., Phan, K., Guo, J., Iancu, L., Weber, J.A., Karger, A., Cain, J.W., Wang, E.C.E., DeStefano, G.M., O'Donnell-Luria, A.H., Christiano, A.M., Riley, B., Butler, S.J., Luria, V., 2020. Apcdd1 is a dual BMP/Wnt inhibitor in the developing nervous system and skin. Dev. Biol. 464, 71-87.

Wada, H., Dambly-Chaudière, C., Kawakami, K., Ghysen, A., 2013. Innervation is required for sense organ development in the lateral line system of adult zebrafish. Proc. Natl. Acad. Sc. U.S.A. 110, 5659-5664.

Wada, H., Kawakami, K., 2015. Size control during organogenesis: Development of the lateral line organs in zebrafish. Dev. Growth Differ. 57, 169-178.

Wang, J., Lu, C., Zhao, Y., Tang, Z., Song, J., Fan, C., 2020. Transcriptome profiles of sturgeon lateral line electroreceptor and mechanoreceptor during regeneration. BMC Genomics 21, 875.

Warth, P., Hilton, E.J., Naumann, B., Olsson, L., Konstantinidis, P., 2018. Development of the muscles associated with the mandibular and hyoid arches in the Siberian sturgeon, *Acipenser baerii* (Acipenseriformes: Acipenseridae). J. Morphol. 279, 163-175.

Winklbauer, R., 1989. Development of the lateral line system in *Xenopus*. Prog. Neurobiol. 32, 181-206.

Wu, D.K., Oh, S.-H., 1996. Sensory organ generation in the chick inner ear. J. Neurosci. 16, 6454-6462.

Yadin, D., Knaus, P., Mueller, T.D., 2016. Structural insights into BMP receptors: Specificity, activation and inhibition. Cytokine Growth Factor Rev. 27, 13-34.

Zhang, X., Xia, K., Lin, L., Zhang, F., Yu, Y., St Ange, K., Han, X., Edsinger, E., Sohn, J., Linhardt, R.J., 2018. Structural and functional components of the skate sensory organ ampullae of Lorenzini. ACS Chem. Biol. 13, 1677-1685.

Zimmerman, L.B., De Jesús-Escobar, J.M., Harland, R.M., 1996. The Spemann organizer signal noggin binds and inactivates bone morphogenetic protein 4. Cell 86, 599-606.

Target Gene	sgRNA	Target Sequence	PAM	Combinations Used
Bmp5	1	TCACGCAGAAAAGCACAGGG	AGG	1+2+3, 1+4
	2	AGATGATGCCTGTTTGCCAG	GGG	1+2+3, 2+3
	3	GGCAAACGAGGAGGAAAACG	GGG	1+2+3, 2+3
	4	GTACAATGCCATGGCAAACG	AGG	1+4
Tyr	1	GGTGCCAAGGCAAAAACGCT	GGG	1+2, 1+2+3+4
	2	GATATCCCTCCATACATTAT	TGG	1+2, 1+2+3+4
	3	GATGTTTCTAAACATTGGGG	TGG	1+2+3+4
	4	GCTATGAATTTATTTTTTTC	AGG	1+2+3+4
	5	GCAAGGTATACGAAAGTTGA	CGG	5+6
	6	GATTGCAAGTTCGGCTTCTT	AGG	5+6
	7*	GGTTAGAGACTTTATGTAAC	GGG	7+8
	8*	GGCTCCATGTCTCAAGTCCA	AGG	7+8

Table 1. sgRNAs used in this study. The target sequences and sgRNA combinations used in this study are shown. The *Tyr* sgRNAs were previously published (preprint, Minařík et al., 2024b); the asterisk against *Tyr* sgRNAs 7 and 8 indicates that these sgRNAs were originally designed and published by Stundl et al. (2022) as their *tyr* sgRNAs 3 and 4, respectively.